UNIVERSITY OF CALIFORNIA
SANTA CRUZ

ON THE ABUNDANCE VARIATIONS OF EUROPIUM IN THE SOLAR NEIGHBORHOOD

A thesis submitted in partial satisfaction of the
requirements for the degree of

MASTER OF SCIENCE

in

PHYSICS

by

Brady D. Lobmeyer

September 2023

The Thesis of Brady D. Lobmeyer
is approved:

Professor Joel Primack, Chair

Professor Natalie Batalha

Researcher Matthew Shetrone

Peter Biehl
Vice Provost and Dean of Graduate Studies

Table of Contents

List of Figures

List of Tables

Abstract

On the Abundance Variations of Europium in the Solar Neighborhood

by

Brady D. Lobmeyer

Europium is a useful proxy in identifying r-process elements such as Thorium and Uranium that act as long-term sources of generated heat in the mantle of terrestrial planets due to their radioactivity and long half-lives. Comparing these abundances to a proxy for the bulk-silicate mantle, such as Magnesium, allows us to describe the geothermal evolution of terrestrial planets. We use stellar data from two independent teams, the first being Delgado-Mena et al. which has 566, out of a total of 1059 stars, having measured Europium values, and the second team being Battistini and Bensby, which has a total of 378 stars, each with measured Europium values. Between these two datasets, there exist only 68 shared stars. With these datasets, we perform an analysis that aims to identify significant star-to-star variation in Europium. Our analysis involves the decorrelation of [Eu/H] values via a metallicity parameter in the form of either [Fe/H] or [Mg/H], as well as Teff while comparing the [Eu/H] vs. Age trend before the decorrelation to the same trend after the decorrelation. For the Delgado-Mena dataset, we perform our analysis twice; first, the individual analysis of the thin disk stars and second, the analysis of the total population according to the galactic populations: thin disk, thick disk, high, and hαmr. The important takeaways from this study are noted as such: the peak-to-peak [Eu/H] values are subject to inflation due to the correlation seen

with both metallicity and Teff parameters. Metallicity parameters impact this inflation greater than the Teff parameter. Teff trends from the separate datasets are of similar magnitude but of different signs, which is indicative of a different problem outside the scope of the purpose of this study. Our analysis of [Eu/H] values after compensating for trends in both Teff and a metallicity term results in a tight dispersion (standard deviation) with these values for the Delgado-Mena data ranging from 0.064 to 0.087 dex. Each of these values is smaller than the quoted average error of 0.1 dex for the raw [Eu/H] values. As for the Battistini & Bensby data, we see the values 0.088 and 0.092 dex, both of which are more consistent with the quoted error of 0.08 dex. Comparing these results to the quadratic sum of the average errors from both datasets with a value of 0.13 dex, tells us that Delgado-Mena is overestimating their errors, whereas, for Battistini & Bensby, the results are inconclusive in determining whether they are over or underestimating. We find evidence for true outliers in the data, with as many as ten stars that exceed 3σ difference for the [Fe/H] & Teff detrended Delgado-Mena data with an average residual [Eu/H] value of 0.17 dex, where we would expect about two outliers for the size of our dataset. Similarly, we find five stars that exceed the same 3σ difference for the [Mg/H] & Teff detrended B&B data with an average residual [Eu/H] value of 0.29 dex. For both datasets, the percentage of stars that exceed the 3σ difference is about 1.5% of the [Eu/H] positive sample size. Averaging the standard deviations from the total population models, we find a [Eu/H] variation value of 0.085 dex which gives us a peak-to-peak range of ± 0.26. What we find is little evidence of significant intrinsic star-to-star variation of [Eu/H]; with peak-to-peak ranges significantly decreased by our

analysis. The motivating literature suggests a range of ±0.5 dex, we find a range of ±0.26 dex, and with relatively few extreme outliers, we are led to believe that the true variation of [Eu/H] is less than the literature suggests.

To my Family,

With much love,

For continuously pushing me to be my happiest self, as well as giving me the tools to pursue my dreams, no matter the trials and tribulations we faced as a whole.

Acknowledgments

I want to thank Mrs. Felardo, my High School Physics teacher, for helping me begin this journey with so much enthusiasm that has made a lasting impact on my view of science as a whole. I also want to thank my committee, Natalie Batalha, Matthew Shetrone, and Joel Primack for their patience as well as the opportunity to pursue this project under their guidance; I am grateful for the chance to work alongside great minds.

Chapter 1

Introduction

1.1 Background

Some important aspects of studying stars and rocky planets alike are the elemental abundances of the star-planet system, as well as the age and effective temperature of the star itself. Each of these aspects is important in understanding the Earth's evolution and finding Earth-like exoplanets. We must first clarify what constitutes an Earth-like planet, and then we can describe the difficulty and importance of searching for other Earth-like planets. An Earth-like planet, by many accounts, is a terrestrial planet that could, given the right conditions, be a home to life. However, as described thoroughly in Rare Earth by Ward and Brownlee [33], the "right" conditions are not trivially defined. It is a list of codependent factors that happen so infrequently that even after a few decades since the first exoplanet was discovered, we are still defining new things that clarify what it is to be truly "Earth-like."

One of the basic ingredients for life as we know it is water in its liquid form, which would require the planet to have a heat source that keeps the surface temperature above 0°C and below 100°C with a similar atmospheric pressure to Earth. Liquid water is an important ingredient, but coupled with it are many more criteria that each contribute to the development of life in different ways. The chances for each of the requirements that would have had to happen at the right time/times in the planetary development, get sequentially lower as more parameters are introduced into the posit of 'what is truly "Earth-like?"'[33] The difficulty of searching for an Earth-like planet is rooted in this complex probability of an increasing amount of factors. An example of this complex probability is the Drake Equation (Eqn. 1.1), in which there are seven parameters that define the probability of finding intelligent life that is capable of communication.

$$N = N^* \cdot f_s \cdot f_p \cdot n_e \cdot f_i \cdot f_c \cdot f_l \tag{1.1}$$

N^* = stars in the milky way galaxy,

f_s = fraction of sun-like stars,

f_p = the fraction of those stars that have planets,

n_e = planets in a star's habitable zone,

f_l = the fraction of planets that could support life that actually develops life at some point,

f_i = the fraction of habitable planets where life does arise,

f_c = fraction of planets inhabited by intelligent beings,

f_l = percentage of a lifetime of a planet that is marked by the presence of a

communicative civilization

Another example is the "Rare Earth" equation (Eqn.1.2) as stated by Ward and Brownlee, which is inspired by the Drake equation but is tabulated for our Galaxy. Where N^* is the number of stars in the Milky Way, f_p is the fraction of stars with planets, n_e is the number of planets in a star's habitable zone, f_i is the fraction of habitable planets where life does arise, f_c is the fraction of planets with life where complex metazoans arise, and f_l is the percentage of a lifetime of a planet that is marked by the presence of complex metazoans.

$$N = N^* \cdot f_p \cdot n_e \cdot f_i \cdot f_c \cdot f_l \tag{1.2}$$

However, if we step back, and attempt to generalize the idea that life comes in many forms, in many different habitats, and could be fundamentally different than anything we have seen here on Earth, then perhaps the definition of an Earth-like planet is slightly more trivial than we would inherently assume.

After considering the probabilistic nature of the likelihood of an Earth-like planet, our first obstacle in our search is the technological challenges we face, which include instrumentation capabilities and the effectiveness of analysis techniques. Our instrumentation capabilities continue to get better; with each new telescope that is built or launched into space, we can look at more of the sky at one time, as well as in more detail than before. However, there are mechanical limits to technology, such as telescope size, as well as the ability to build/maintain space telescopes. With the prospect of adaptive optics, we can tackle a few problems that appear for large

traditional (ground-based) telescopes, such as the fact they require perfectly sculpted glass lenses/mirrors of massive size, as well as the hindrance introduced by atmospheric interference. Where adaptive optics allows for a large telescope to be composed of smaller pieces and can account for atmospheric interference in such a way that reduces the uncertainty in measurements. As for space telescopes, with the advent of the James Webb Space Telescope (JWST), we have upgraded our capabilities in searching the cosmos for another Earth, with the potential of directly imaging exoplanets [9]. When it comes to analysis techniques, we continue to optimize them with time, as well as the realization of new techniques with more modern technology. With each breakthrough, either in technology or analysis, we gain a better understanding of the universe, and in turn, we develop a better understanding of Earth and the planets that are much like it.

Earth-like planets are important to search for, so we can better understand the prevalence of the conditions that we understand to be needed for the sustainability of life. Big surveys looking for potential Earth-like planets only give bulk properties, i.e., mass, radius, etc. They look at planets in habitable zones, but it requires more detail to determine if the planets have habitable environments. The majority of exoplanets found in big surveys are Super-Earths/Mini-Neptunes [15], which highlights the difficulty in identifying terrestrial planets that are a primary focus of searching for exoplanetary life. We can only estimate how common terrestrial exoplanets are and, in a similar vein, how common terrestrial moons of exoplanets are. What we do know is that more exoplanets are being found, and our job is only beginning in understanding these objects.

What we can do in the search for habitable exoplanets is take the abundance

analysis of stars, which tells us the fractional composition of elements, and since planets are composed of similar materials as their home stars [31], this then allows us to model the interior composition of planets effectively. From this modeling, we can better understand the terrestrial planets and how they would have evolved. This idea is where this project takes inspiration from. In looking at our current understanding of radiogenic element abundances, we wanted to understand better how these elements fit into the search for Earth-like planets.

1.2 Motivation

Nimmo et al. (2020) [23] notes that the abundance of radiogenic elements is a crucial factor in how Earth evolved. The reason for this is that terrestrial planets like Earth are heat engines, and the heat they generate comes from three sources, the first being gravitational energy released as the planet formed, which corresponds to a value of around 40 MJ/kg for an Earth massed body [23]. The second is tidal heating which produces 3.7 Terawatts(TW) due to the Earth, Moon, and Sun system, where the Earth-Moon system is about 95% of the heat production [20]. Whereas the last is the decay of radioactive elements, and for Earth, the estimated amount of energy from formation to now is around 1 MJ/kg [23]. If we compare the two heat rates, it would require a few ten-billion years for tidal heating to produce as much heat as has been produced from radiogenic heating. The heat produced drives internal processes such as magnetic dynamo generation, volcanism, and plate tectonics via the thermal processes

of conduction, convection, and advection [23]. Tidal heating and radiogenic heating are long-term sources of the thermal evolution that has made Earth what it is today.

Tidal heating is a relatively simple process that involves two or more objects orbiting their respective center-of-mass, which can cause tidal forces that produce heat in a calculable manner, whereas radiogenic heating is much more involved as it requires modeling various sources of radioactive decay simultaneously over a long time period. It accounts for the majority of current heat production in Earth's interior, more specifically the mantle and crust, which could be critical for life. The reason for this criticality is twofold; firstly, the long-lived radiogenic heating would keep the mantle hot enough for convective currents of magma that cause tectonic plate movement, which is important for geological evolution, which also assists magnetic dynamo generation that allows the existence of Earth's magnetic field. Secondly, as a byproduct of the long-term geological evolution in the form of tectonic plates, which is theorized to help biodiversity, which increases survivability, it happens to allow life to have the ability of trial and error [33]. As described in Rare Earth, life as we know it today required billions of years to develop; with multiple extinction events that, were it not for the biodiversity introduced due to the active tectonics reshaping the land and water habitats, life surely would have come to a halt. A side-effect of tectonic plate movement is that it is a significant source of heat loss, such that the heat lost is double that of the heat generated by the dynamo [23]. This heat loss associated with tectonic plates can be beneficial to maintaining a long-term dynamo, as too much heat can suppress the magnetic dynamo to the point where it no longer acts as efficiently if at all [22, 21, 31, 24].

In order for radiogenic heating to occur, there needs to be a significant amount of the radioactive isotopes of Potassium(^{40}K), Thorium(^{232}Th), and Uranium(^{235}U & ^{238}U), as these three elements are the biggest contributors to long-term produced heat due to their long half-lives. K is a volatile element that is produced in type II supernovae [25] and s-process nucleosynthesis [29] with a half-life of $1.25*10^9$ years. The volatility of an element means that during planetary formation/accretion, it is susceptible to being lost, which makes the abundance tracking more difficult [16]. In our own solar system, there exists a large variation of K in between the terrestrial planets [18]. As for U and Th, where U has a half-life as long as $\sim$4.5 billion years, and the most common isotope of Th has a half-life of 14 billion years, with other isotopes having significantly shorter half-lives and, as a result being less prevalent. These elements are less likely to be lost during the accretion stage, where it is expected that the surrounding terrestrial planets will retain a similar ratio of these elements with their star [23, 31].

Two types of neutron capture processes are relevant when looking at elements heavier than iron, the first being the aforementioned s-process (slow-process) and the second being the rapid-process (r-process). Neutron capture is the process in which elements are bombarded with neutrons, but the 'slow' and 'rapid' terminology comes from the comparison to the β-decay rate. In the r-process, the neutron capture happens before β-decay can occur, whereas, in the s-process, neutron capture happens so infrequently that it allows the element to stay within the β stability valley. The s-process occurs in lower-mass AGB stars as well as during the Helium (He) burning stages of the stellar evolution of high-mass stars. There are two origins for the s-process that produce

elements such as Barium (Ba), and Cerium (Ce) for heavy s-process and Strontium (Sr), Yttrium (Y), and Zirconium (Zr) for light s-process [3, 12]. These can occur over long periods of time, where the r-process happens in special cataclysmic events that occur on much shorter timescales. The source of r-process elements has been a highly debated subject for many years [6, 23, 30].

When it comes to Th and U, they are r-process elements that are most likely created via the rare event of neutron star mergers [23]. These events produce large amounts of r-process elements and are infrequent enough to cause the expectation of considerable variation in the galactic abundances of these elements. When it comes to measuring the abundances of Th and U, it is easier to use a proxy element due to these elements being difficult to identify via spectral analysis due to blending and the decay of ^{235}U [7, 26]. Europium(Eu) is our proxy as it is the most common proxy for the radiogenic elements, as they are all r-process elements, and Europium is much clearer when spectrally analyzed [7, 23, 26]. We show the spectral lines for Eu II, Th II, and U in figure 1.1 detailing the reasoning behind using Eu as a proxy element due to Eu's prominent individual lines as well as highlighting the difficulty that arises when trying to observe unique lines in the spectrum for the Th II and U [14].

A figure (1.2) from Nimmo et al., 2020 [23] describes what the thermal evolution models predict as we change the fraction of radiogenic elements. We see that at higher values of the initial fraction of radiogenic elements, we are at a greater risk of not producing a dynamo for an increasing amount of time as the fraction rises. This is exemplified by the top red line (labeled Fig 1c), which has 3 times Earth's initial U and

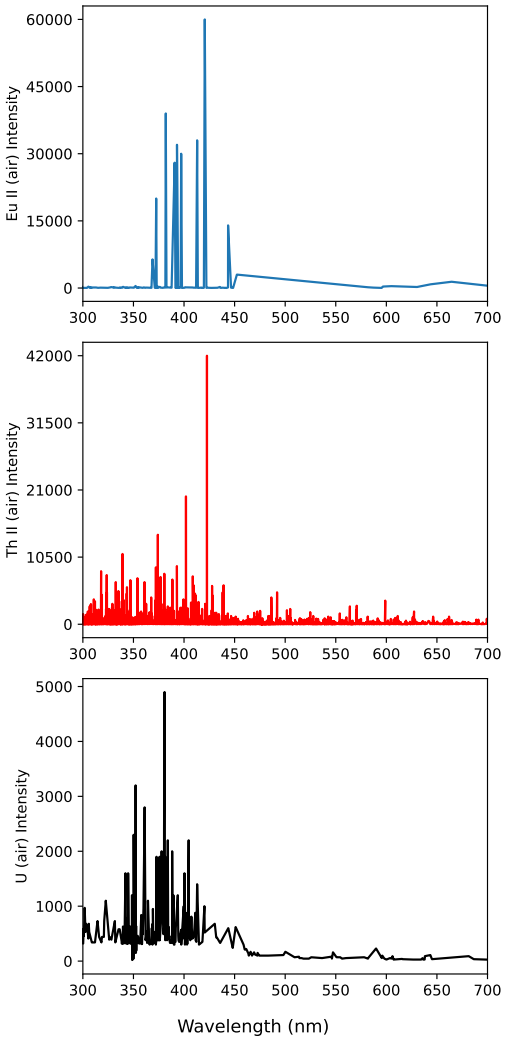

Figure 1.1: Spectral lines of Eu II (blue), Th II (red), and U (black) in air. The three plots detail that Eu is an ideal choice for spectral analysis due to the prominent intensity and gaps between most of the lines, whereas Th and U do not contain these gaps for many of their lines and, thus, are more difficult to isolate especially when other element lines are present (i.e., in an unfiltered spectrograph).

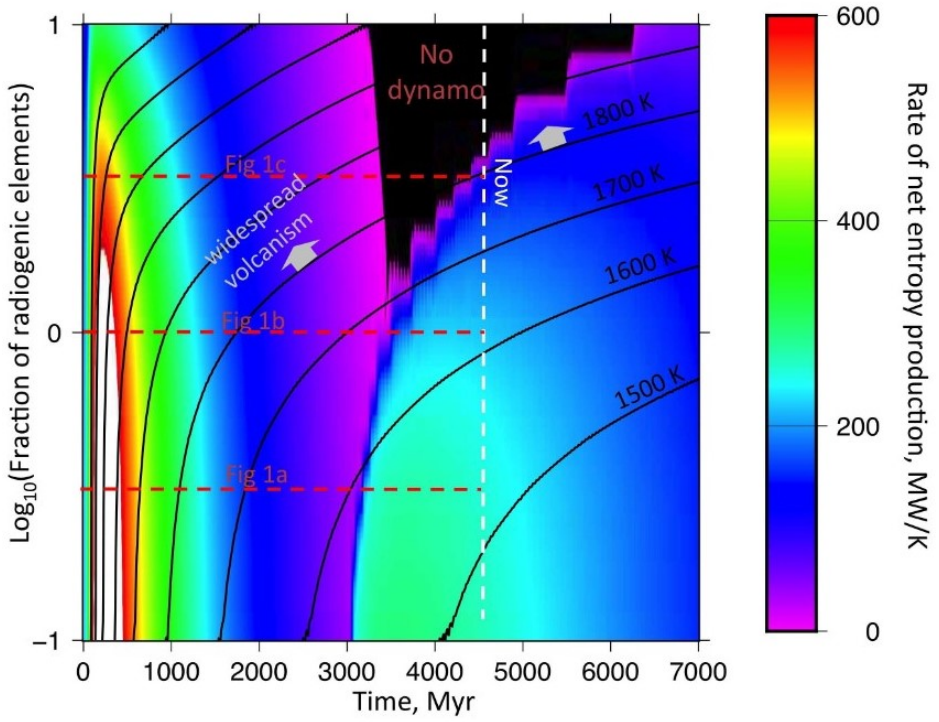

Figure 1.2: A reproduced figure from Nimmo et al.[23] showing the effect that the initial fraction of radiogenic elements, in the form of U and Th, has on the rate of entropy production in Mega Watts per Kelvin over the planetary lifetime scale in Millions of years (Myr). The three dashed red lines are the trajectories of different evolution models, and the white dashed line corresponds to the present day. The black region corresponds to a negative rate of entropy production, while the colors correspond to the color bar on the right. The black lines represent the mantle's potential temperature.

Th abundance. We also note that at a lower initial fraction (0.3 times Earth's on the bottom red line labeled Fig 1a), we produce more entropy due to a ∼2000 Million year wide spike of higher entropy production, which results in less time spent producing very little entropy (pink region). If we look at the middle red line (labeled Fig 1b), which is the Earth analog, we note that it produces entropy at a modest rate that prevents it from evolving into a "no dynamo" system, but it does result in higher core potential temperature than the low fraction case.

When creating a thermal evolution model, heat production is important; however, terrestrial planets are composed of many things, not only radiogenic elements but silicates as well, and a basic understanding of thermodynamics tells us that heat propagates differently through different materials, which we must account for when modeling thermal evolution by modeling the heat propagation. The parameter we use to model the heat propagation is known as bulk silicate mantle, which is a generalized measurement of the silicate abundance found in the mantle. The bulk silicate mantle can be modeled using a proxy element, which is commonly chosen in thermal evolution models as Magnesium(Mg) or Silicon(Si) [23]. We choose to look at Eu in relation to Iron(Fe) and Mg.

We look at the Fe case for a couple of reasons, the first being to stay consistent with the convention of the papers we chose data from. Our second reason is so we can compare our findings in the Fe case to the Mg case. As for the Mg case, Mg is an alpha element, and as such, it is neither volatile nor subject to the high variability seen in r-process elements. Mg is simply chosen due to the observed stellar Mg/Si ratios showing

only tens of percent variability, which is to say we could have chosen either element and would expect similar results [8]. However, to model the bulk silicate mantle, we need a better understanding of chemical evolution and the abundance trends of the stars, which can vary depending on their galactic radius and age.

Tsujimoto [30] looks closely at the galactic radius as a key factor in the metallicity of stars, according to the hypothesis that chemical enrichment is greater with a decreasing galactic radius. Tsujimoto's work also aims to suggest that the r-process elements are produced by two different sites, one being the case of neutron star mergers and the other being short-lived massive stars with specific core-collapse supernovae [30]. Both of these factors are important for our analysis and understanding of our results. Understanding that the r-process elements could come from two different sites helps us understand the relationship between element abundance and age. However, we do not take into account the stars' measured galactic radii; we do note the galactic population the stars lie in, i.e., the thin or thick disk, as well as the high alpha metal-rich (hαmr), and the halo populations for one of our datasets [1]. If further analysis of each of the stars' galactic radii is accounted for, we could potentially provide clearer conclusions about the abundance properties. Tsujimoto's study is limited by a small sample size of 79 solar twins used by Bedell et al., 2018 [30, 4]. Using solar twins has its benefits, with the idea that no systematic biases, such as differences in temperature, mass, composition, etc., are introduced. This is needed due to the analogous nature that the stars have with our well-studied Sun, and the errors on most of the parameters of interest are significantly smaller than those of stars not considered to be a solar twin [4]. Bedell et

al. [4], however, finds that the Sun has an anomalous abundance trend when compared to most of these twins. This is important to note, for if we are to pair this information with Kepler's statistics of exoplanetary systems, we can infer that a good categorization of stellar abundances would help us narrow the search for Earth-like exoplanets, which coincides with our overall goal as stated at the end of this section.

We look at the Delgado-Mena et al. data from their 2019 paper as well as their 2017 paper which looked more closely at the raw abundances than the 2019 paper [11, 12]. We chose their data because it has a high resolution (R $\sim$ 115000) and high-quality spectra from the HARPS-GTO program. Similar to what Griffith et al. did, we compare this data to the Battistini and Bensby(B&B) data [13]. The reason we compare the datasets is to increase our sample size, as well as to identify any significant differences in their results after we have performed our own analysis of their data. Our analysis looks at the various relationships seen when compared to the [Eu/H] abundance, where we perform systematic detrending of effective temperature (Teff) and/or [Fe/H] or [Mg/H]. The initial [Eu/H] abundance distribution seen in the Delgado-Mena (DM) data can be seen in fig 1.3 and similarly for the Battistini and Bensby data in fig 1.4. Where we adopt the standard spectroscopic notation used in Afşar et al. [2] that originates from Wallerstein and Helfer [32], that for elements A and B, [A/B] $\equiv$ $\log_{10}(N_A/N_B)_* - \log_{10}(N_A/N_B)_\odot$. Using the definition log $\epsilon(A) \equiv \log_{10}(N_A/N_H) +$ 12.0, and equate our metallicity terms with the stellar value. The causes of the breadth in the distributions of the data could be attributed to either metallicity source Fe or Mg, effective temperature, stellar age, systematic biases, star-to-star scatter at a fixed

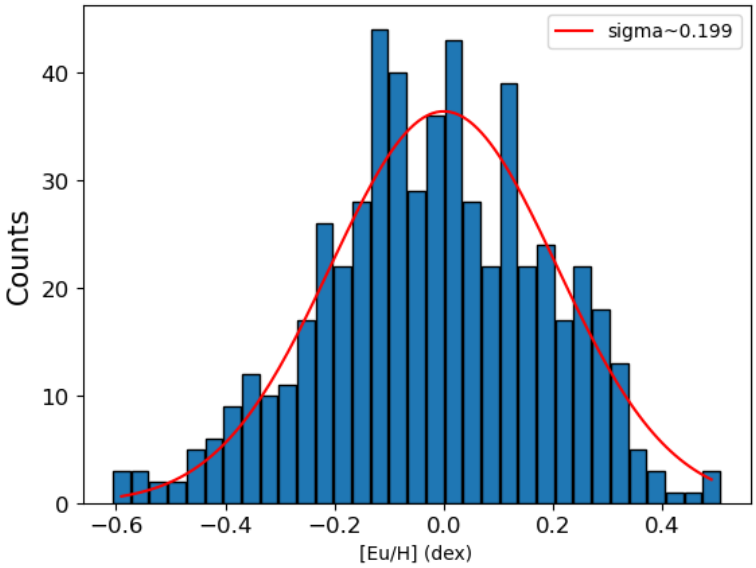

Figure 1.3: Histogram of the raw Delgado-Mena [Eu/H] abundance values for the total population of stars. The red line depicts a Gaussian best-fit line to the data with the corresponding standard deviation denoted as sigma. The typical error for these [Eu/H] values is ∼0.1 dex

metallicity, as well as perhaps many other factors that are beyond our focus.

The short-term objective of this paper is to quantify the star-to-star differences in [Eu/H] abundances before and after detrending against Fe, Mg, and effective temperature. This objective is a step in the direction of our overall goal to understand better the diversity of terrestrial exoplanets, which will assist in the search for life and/or habitable exoplanets that are nearby, including those in the Kepler demographic sample.

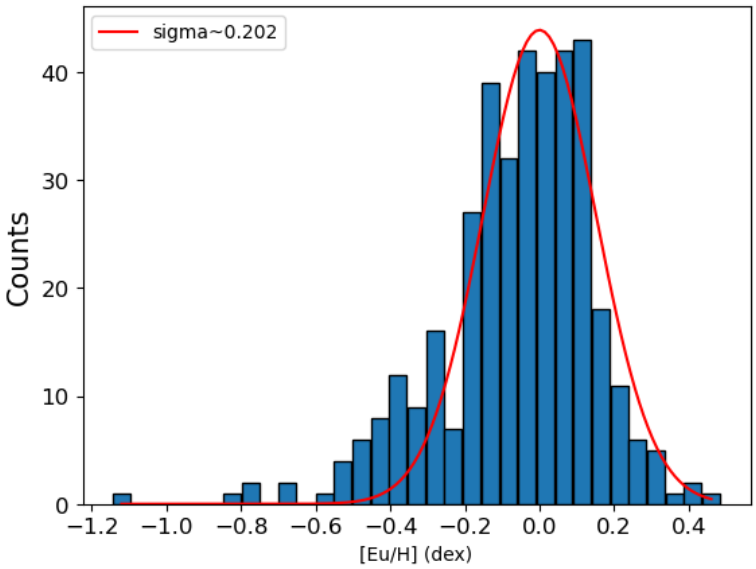

Figure 1.4: Histogram distribution of the B&B Raw [Eu/H] values. The red line is a Gaussian best-fit line with a corresponding standard deviation denoted by sigma. The quoted error for [Eu/H] in this dataset is 0.08

Chapter 2

Methods

2.1 Data

We re-analyze the Delgado-Mena data due to the large dispersion of Eu abundances included in the Hypatia catalog as noted by Nimmo et al. [23], as well as, to better understand the characteristics of the Europium abundance ([Eu/H]) as a function of age. Age holds importance here due to the chemical evolution of Eu, and we want to know if it tracks with Fe and/or Mg hence why we detrend the relationships by Fe or Mg. We perform the analysis of the Delgado-Mena data by visualizing the data in histograms and scatter plots. The scatter plots are of the [Eu/H] abundances against another abundance term ([Fe/H] or [Mg/H]), effective temperature (Teff), and finally, age. We perform a nearly identical analysis of the Battistini and Bensby data, where the only difference lies in the availability of what population the stars inhabit. For the Delgado-Mena data, this information is available, allowing us to categorize the stars into

each of the populations; this is not inherently the case for the Battistini and Bensby data. With the population information available, we chose to look at how the total population acted according to our analysis as well as how the thin population acted to the analysis.

We statistically analyze the plots to develop models that allow us to detrend the [Eu/H] abundance in one or two dimensions in order to determine if age by itself is an effective tool to determine the relative abundance of the stars. Detrending against one of our abundance terms or Teff individually is our one-dimensional detrend, and this allows us to test the individual effects on the abundance trend against the opposite term; for example, if we detrend Teff, we then compare [Eu/H] to [Fe/H] or [Mg/H] and vice-versa. Whereas the two-dimensional detrending model is the combination of both the Teff and one of the abundance parameters being eliminated from the abundance vs. age relationship. This allows us to view the combined effects on the abundance vs age relationship.

After we display the [Eu/H] trends on their scatter plots, we look at the distribution of the [Eu/H] values before our detrending and the [Eu/H] residuals which are the resulting values from the detrending analysis. We perform a Gaussian best-fit approximation to understand the standard deviation of the distribution. Alongside the Gaussian best fit, we perform a KS test that tells us the statistical significance of the histograms, as well as whether they are normally distributed or not. For the Delgado-Mena data, we show the [Eu/H] abundance for both the total and thin populations, corresponding to both versions of the 2D detrending, which are denoted by

either [Fe/H] or [Mg/H].

We also look at the relationship our detrended [Eu/H] values have with the quoted error. We look at the Fe detrending for the Delgado-Mena dataset to convey this relationship for the reason that Fe is a common property for which bulk surveys search [27]. As for the B&B dataset, we look at the Mg detrending, where we expect similar but slightly different results to those seen in comparison to the detrending of Fe from [Eu/H]. We do this by taking the residual [Eu/H] and dividing it by the errors associated with that measurement, where we then compare it back to the same residual [Eu/H] values. This allows us to look at how effective the quoted errors are and could help determine if the quoted errors are either over-estimated or under-estimated. We do this for both datasets; however, for the Battistini and Bensby datasets, there exists a single quoted error rather than associated errors for each measurement seen for the Delgado-Mena dataset.

2.2 Equations

Initially, the abundances from Delgado-Mena were in a different format, in which we used equations 2.1 and 2.2 to convert them to a more understandable format and equations 2.3 and 2.4 are for the error propagation.

$$[Eu/H] = [Fe/H] + [Eu/Fe] \tag{2.1}$$

$$[Mg/H] = [Fe/H] + [Mg/Fe] \tag{2.2}$$

$$[Eu/H]_{Er} = \sqrt{[Fe/H]^2_{Er} + [Eu/Fe]^2_{Er}} \tag{2.3}$$

$$[Mg/H]_{Er} = \sqrt{[Fe/H]^2_{Er} + [Mg/Fe]^2_{Er}} \tag{2.4}$$

The idea for this format is for it to be more comparable to the metallicity parameter [Fe/H]. After converting to this new format, we wanted to look at the distributions and test whether they follow a linear trend or not. To do this, we use a Pearson test that gives a correlation coefficient and a two-tailed p-value. We cross reference the p-value by converting the correlation coefficient into a T-score via equation 2.5, then we convert the T-score into a p-value using a conversion calculator. We find that these two p-values are the same for each relationship.

$$T = r\sqrt{\frac{n-2}{1-r^2}} \tag{2.5}$$

Our hypothesis is that there is a linear trend between the parameters we are interested in, more specifically, the [Eu/H] abundance and age. Our chosen significance level is that of 3σ, which can also be stated via the "alpha level"($\alpha = 0.001$) where a p-value less than α signifies that our hypothesis is reasonably believable. If the p-value is greater than α, we cannot accept that our hypothesis is correct and would expect a different relationship may be present or that our analysis removed a factor that made the relationship significant. In the case of our p-value being greater than alpha, a remedy to this problem might require more data to come to a more definitive conclusion.

In the next section, we show the results of analyzing the data via graphs that show the relationship [Eu/H] has with the other parameters before and after detrending. The detrending process uses simple equations utilizing values acquired from the data analysis. For our 1D detrending, we use equations 2.6 and 2.7 separately to test the

effects they have on the [Eu/H] vs age relationship. Equation 2.8 is what we use to detrend in two dimensions.

$$[Eu/H]_{Resid} = [Eu/H] - (y_{int} + m \cdot ([Fe/H] or [Mg/H])) \tag{2.6}$$

$$[Eu/H]_{Resid} = [Eu/H] - (y_{int} + m \cdot T_{eff}) \tag{2.7}$$

$$[Eu/H]_{Resid} = [Eu/H] - (y_{int} + m_1 \cdot ([Fe/H] or [Mg/H]) + m_2 \cdot T_{eff}) \tag{2.8}$$

The y-intercept and slope (m) parameters are acquired from the initial relationships of [Eu/H] against their respective parameters (i.e., metallicity or Teff). For equation 8, we used a two-dimensional line model to fit the data, and we used the resulting slopes and intercept, where the slope corresponds to the parameter value we are multiplying by. For example, if 'm' is being multiplied by Teff, it then corresponds to the slope seen in the [Eu/H] vs Teff relationship. We choose to call the detrended [Eu/H] values the 'Residual' values, as it represents the relationship that survives the detrending process.

The data has a rich concentration of thin disk stars, so we decided to model the thin disk individually, separate from the other star populations. The other populations, as stated before, are the thick disk, high alpha metal-rich, which are based on their [α/Fe] separation (α is the average of Silicon, Magnesium, and Titanium) over different metallicity bins, and halo populations which are defined based on their kinematics [11, 12, 1]. The total model is a combination of all the populations, in which we choose not to display the thin disk stars when describing the total model trend. The reason we

include the thin population in the total model is that it has more values than the other three populations combined, whereas if we were to model the other three populations by themselves, they would not be significant due to the amount of data available. The reason the thin disk stars are not present in the total model graphs is that we wanted to be able to show the effect that the other populations have on the thin model trend without sacrificing the clarity of the plots. If the thin disk stars are present in the total model distributions, it is more difficult to visually identify the other populations and their effects on the trends.

We rearrange equation 2.8 to a form seen in equation 2.9. Doing this allows us to understand our results in the context of Fig 1.2, where we now have the ratio of our radiogenic element proxy to the silicates proxy. The m_1 is the slope corresponding to the [Mg/H] slopes in Table A.2, which are the same values used in the detrending equations. The star-to-star scatter portion of this formula is the $[Eu/H]_{res}$ term in which we choose to use the resulting standard deviations of our analysis as the value.

$$[Eu/Mg] = (m_1 - 1) \cdot [Mg/H] + [Eu/H]_{res} \tag{2.9}$$

When we plot the histograms of the various [Eu/H] relationships, we check if the variance of our data is distributed normally. We do this via a Gaussian of the form seen in equation 2.10. The standard deviation is found by taking the square root of the variance of the [Eu/H] data and is the value denoted as sigma in the histogram plots.

$$Gauss = A \cdot e^{-bx^2} \tag{2.10}$$

Chapter 3

Results

3.1 Delgado-Mena

The results of our analysis of the Delgado-Mena dataset are depicted in the graphs below. In total, we find a set of 566 stars that are Eu positive (Eu positive: Eu was detected spectroscopically) in the Delgado-Mena data; this is further split into different sub-sets that contain the following values: Thin=453, Thick=71, Hαmr=40, Halo=2. For Figures 3.1 to 3.8, the left plots are of the thin distribution, and the right plot is that of the total distribution, with the thin stars excluded visually. The lines have their parameters listed in their corresponding boxes and colors, as noted in the figure descriptions.

First impressions from Fig 3.1 imply an important relationship between [Eu/H] and age. The trend we see implies that the older stars viewed in the HARPS project data have less [Eu/H] compared to the younger stars. Another aspect we see is the

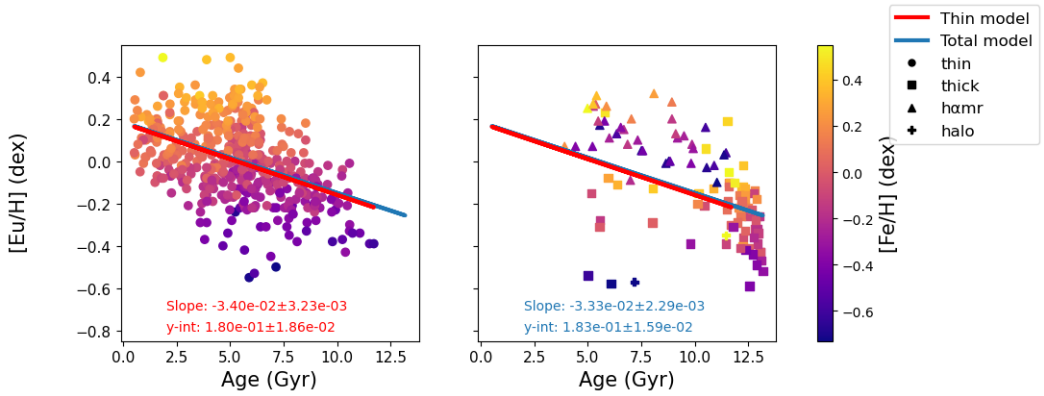

Figure 3.1: [Eu/H] as a function of stellar ages with a [Fe/H] distribution bar. (left) Thin distribution with the linear fit in red, with its corresponding parameters in red. (right) Thick, hαmr, and halo stars are shown as denoted by the legend, with the linear fit line to all of the data, including the thin sample, as well as its corresponding parameters in blue. The P-values for both plots are less than α; this tells us they are acceptable models.

minimal difference between the trends of the thin population and the total population, which likely is because of the weight the thin population has on the trend line due to the amount of data available. If we were to model any of the other populations by themselves, we would expect to see large differences in the trend line, which again is due to the limited dataset. These aspects are important in moving forward, as they can shape our understanding of future plots. Continuing forward, we want to look at the relationship [Eu/H] has according to Teff and [Fe/H], to detrend according to each individually, and then both to test if it has any apparent effects on this relationship between [Eu/H] and Age.

In Fig 3.2, we show how the [Eu/H] trends against [Fe/H] before we detrend, implying a positive correlation between the two parameters. An important result from this relationship is that the slope is less than one, which tells us that Eu tracks closely

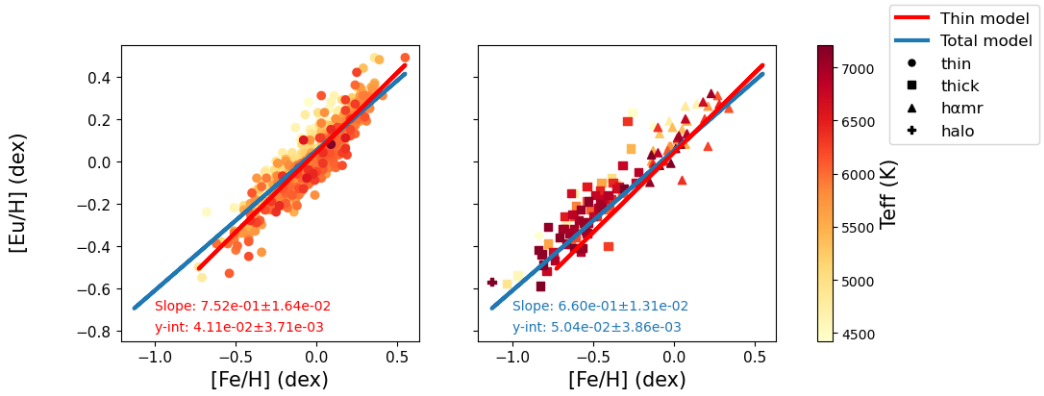

Figure 3.2: [Eu/H] as a function of [Fe/H] with a Teff distribution bar. (left) Thin distribution with linear fit and parameters in red. (right) Thick, $h\alpha$mr, halo distribution where the symbols are shared from 3.1. The P-values for both plots are less than α; this tells us they are acceptable models.

with Fe, which is beneficial in our understanding of galactochemical evolution. From this figure, we infer that the sources producing Fe do so in greater amounts as the metallicity increases compared to the sources producing Eu. Since this is a prominent relationship for [Eu/H], we want to test how it affects other relationships, starting with the relationship [Eu/H] has with Teff.

Eliminating the [Fe/H] trend seen in fig 3.2 lets us convey the results in such a way that allows us to better isolate the relationship that [Eu/H] has with Teff as shown in fig 3.3. The residual trend for [Eu/H] against Teff implies a negative correlation, which is to say that the hotter the star, the lower the [Eu/H] ratio is expected. This relationship is peculiar, as it does not make much sense, Eu is an r-process element that is not created in the lifetime of a star, except for maybe the end [30]. Although interesting, we discuss this result in section 4. Moving forward, we choose not to show the Teff detrended plots due to the minimal change seen between the original and detrended

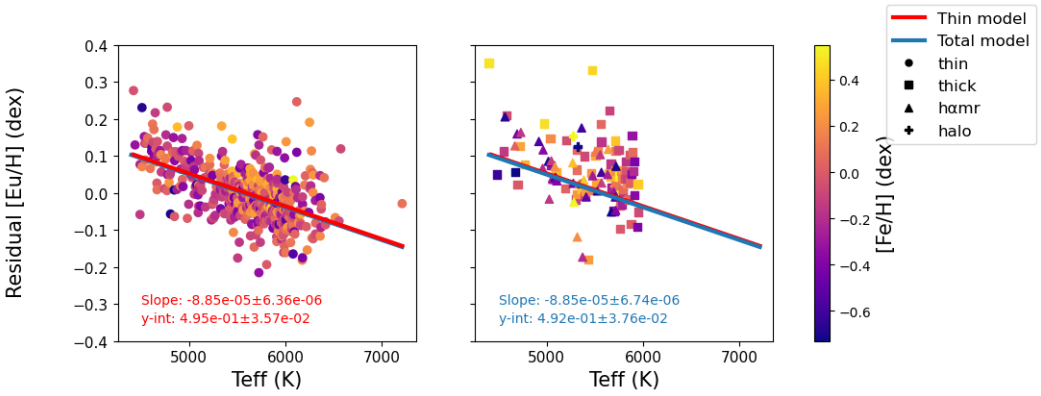

Figure 3.3: [Fe/H] Detrended [Eu/H] as a function of Teff with a [Fe/H] distribution bar. (left) Thin distribution with linear fit and parameters in red. (right) Thick, hαmr, halo distribution where the symbols are shared from fig 3.1 The P-values for both plots are less than α; this tells us they are acceptable models.

graphs, which tells us that temperature has very little influence on the metallicity of a star, which can be inferred from the seemingly random distribution of stars when comparing it to the [Fe/H] color bar.

In figure 3.4, we eliminate the [Fe/H] and Teff trends, where we again look at the relationship that our (now residual) [Eu/H] abundances have with age. Comparing back to fig 3.1 for the total population, we see a sign change from a negative to a positive trend in the slope. As for the thin population, we find that it still has a negative correlation; only its magnitude has decreased by nearly a full factor of ten. However, we cannot look too closely at this due to the fact that these trend lines are not significant. This tells us that one/or both of our detrending parameters had an effect on the [Eu/H] vs. Age relationship.

When looking at individual detrending processes not shown here, we find that the Teff detrend caused a minimal change in the slope of the [Eu/H] vs. Age relationship,

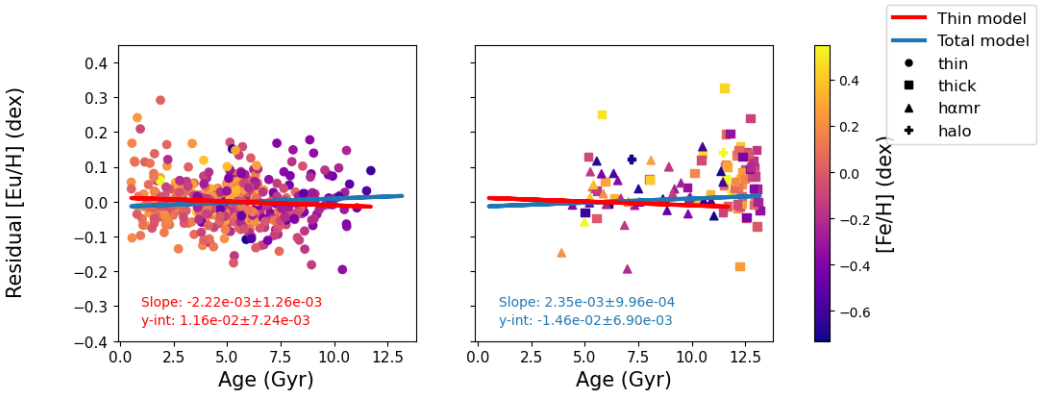

Figure 3.4: Teff and [Fe/H] Detrended [Eu/H] as a function of stellar Age with a [Fe/H] distribution bar. (left) Thin distribution with a linear fit and parameters in red. (right) Thick, hαmr, halo distribution where the symbols are shared from fig 3.1. The P-values for both plots are greater than α, which means we cannot accept these models initially.

causing it to be slightly more negative, where detrending against [Fe/H] made the relationship positive. Perhaps the combination of the two parameters we detrend by is the source of the discrepancy in the slopes of the different population models. For these models, we note that the P-values are not within our accepted range; we believe the reason this is the case is due to the similar evolutionary timescales seen in Eu and Fe. It is for this reason that eliminating the Fe trend for this specific relationship causes the models not to meet our statistical significance standards.

It is important to describe the [Eu/H] abundance and its correlation to age when accounting for the [Mg/H] abundance as well. Doing this allows us to understand if the relationship we see between [Eu/H] and age relies on [Mg/H] as we saw in fig 3.4 when we looked at Fe's and Teff's relationship to this trend. It is also important for another reason, which is the fact that we are hoping to categorize the Eu abundance in such a way that allows us to better understand the terrestrial planets surrounding

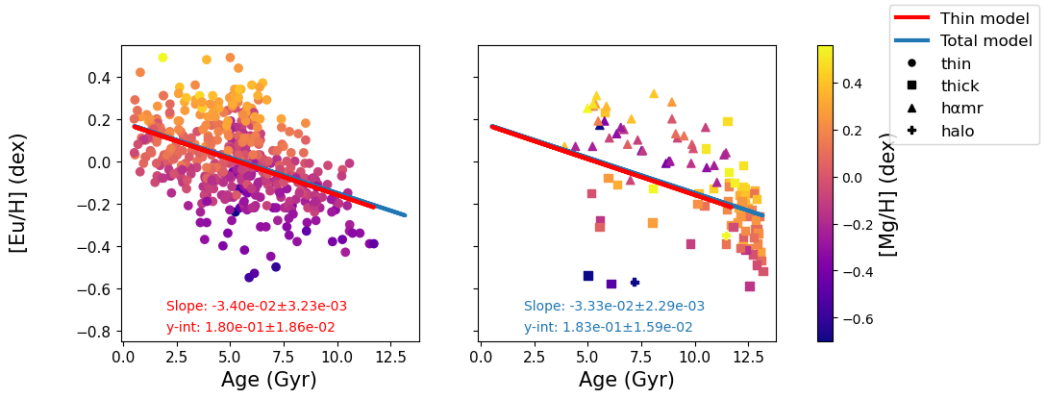

Figure 3.5: [Eu/H] as a function of stellar Age with a [Mg/H] distribution bar. (left) Thin distribution with a linear fit and parameters in red. (right) Thick, hαmr, halo distribution where the symbols are shared from fig 3.1 The P-values for both plots are less than α; this tells us they are acceptable models.

stars. In order to do that, we need to model the bulk-silicate mantle of these planets, which we do with the Mg abundance. This marks the beginning of our Mg analysis for the Delgado-Mena dataset, in which we show plots similar to those seen in figures 3.1, 3.2, 3.3, 3.4, where instead of looking at [Fe/H] we look at [Mg/H] and its effects on [Eu/H]'s relationships.

In figure 3.5, we see the same physical distribution seen in Fig 3.1; however, as noted before, the color-bar is different as it depicts the [Mg/H] distribution rather than the [Fe/H] distribution. This plot does show that the [Mg/H] acts similarly to [Fe/H], which we show in more detail in fig 3.6.

For fig 3.6, we see similar results seen in fig 3.2, where Eu tracks closely with Mg at around the same rate it tracks with Fe. Since Fe and Mg act similarly when compared directly to Eu, it allows us to compare the differences seen between the respective detrended data. We would expect similar results to the Fe case in our detrending

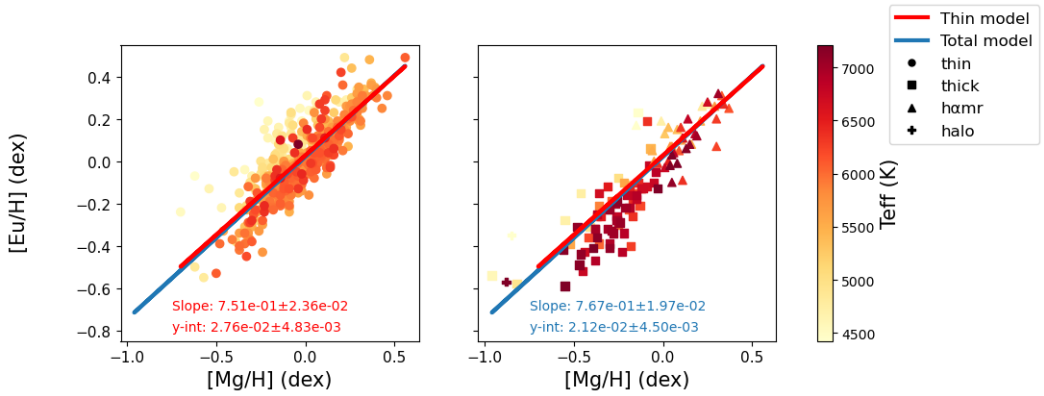

Figure 3.6: [Eu/H] as a function of [Mg/H] with a Teff distribution bar. (left) Thin distribution with linear fit and parameters in red. (right) Thick, hαmr, halo distribution where the symbols are shared from fig 3.1 The P-values for both plots are less than α; this tells us they are acceptable models.

process, this is not the case, however, and we do see some significant differences in the figures 3.7 and 3.8 when we compare back to figures 3.3 and 3.4 respectively.

For fig 3.7, we see a negative correlation for the residual [Eu/H] vs Teff; however, when we compare to fig 3.3 we see that the slope is greater in magnitude when detrending against [Mg/H] vs a smaller magnitude when detrending against [Fe/H]. Much like fig 3.3, we find this relationship to be peculiar for the same reasons and will probe further in a later section. We move forward to compare the effects the two-dimensional detrending has on the [Eu/H]-age relationship while accepting the models we detrend with due to their statistical significance being in our accepted range, where we result in fig 3.8.

For figure 3.8, we see a persistent negative correlation seen in our raw trends; however, it has increased by nearly a full order of magnitude. When we compare this to the results shown in 3.4, we see that the Fe detrending had a more significant effect

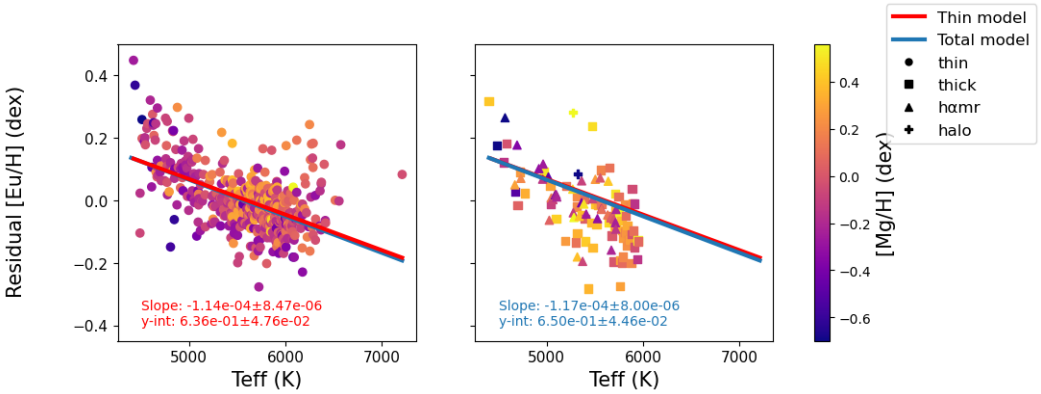

Figure 3.7: [Mg/H] Detrended [Eu/H] as a function of Teff with a [Mg/H] distribution bar. (left) Thin distribution with linear fit and parameters in red. (right) Thick, hαmr, halo distribution where the symbols are shared from fig 3.1. The P-values for both plots are less than α; this tells us they are acceptable models.

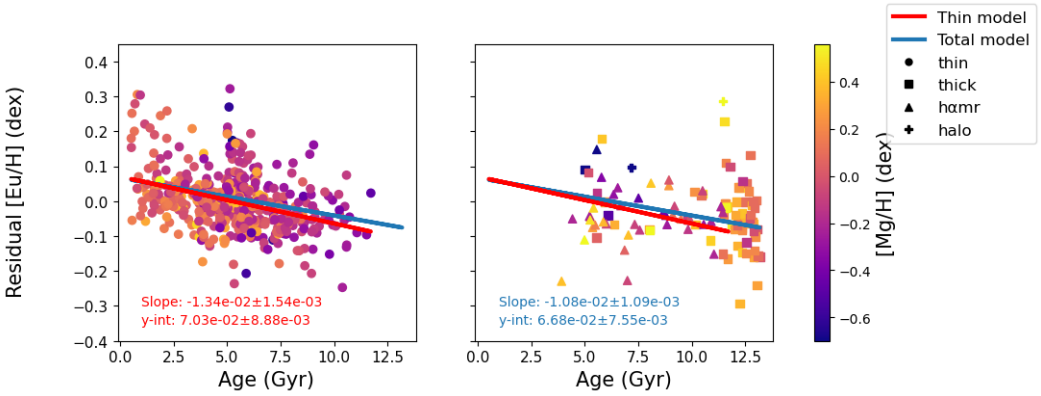

Figure 3.8: Teff and [Mg/H] Detrended [Eu/H] as a function of stellar Age with a [Mg/H] distribution bar. (left) Thin distribution with linear fit and parameters in red. (right) Thick, hαmr, halo distribution where the symbols are shared from fig 3.1 where we see a significant change in the slope from figure 3.5. The P-values for both plots are less than α; this tells us they are acceptable models.

on the age trend than the Mg detrending did. This is interesting, considering the idea that Eu tracks age similarly to Fe, whereas Mg does not track age as well, telling us that when comparing Eu to Fe, age can be disregarded, but when comparing Eu to Mg, age is a factor that should be included. To have the differences we see means that there is an underlying correlation between some of the parameters that we have not fully accounted for.

Considering that the P values from figure 3.4 are not in our accepted range and that the P values from figure 3.8 are in our accepted range, where the only difference between the two is by what element we detrended by, we can begin to postulate what correlations may be behind this observation. From our analysis, we believe that it would be a safe assumption to rule out Teff as the cause of this difference in our statistical acceptance due to figures 3.4 and 3.8 both being detrended by Teff and since it has very minimal effect on the slope of the [Eu/H] vs. Age graphs. In order to develop our understanding of the differences, we take the opportunity to directly compare the [Eu/H] distributions both before and after detrending.

We showed figure 1.3, which looks at the initial distribution of [Eu/H] abundances for the Delgado-Mena data in the introduction. This distribution gives us a baseline to compare to when looking at the detrended versions of the distribution. Testing the distribution of the residuals from figures 3.4 and 3.8 in figures 3.9 and 3.10, we first note each of the distributions looks asymmetrical and then is determined to be non-normal according to the results of a KS-test. We can also observe the differences in the overall dispersion from before and after our analysis process, which results in much

smaller ranges in which the [Eu/H] values inhabit. This tells us that [Eu/H] is susceptible to being over/underestimated due to the relationships held with other parameters. This aspect leads us to a similar comparison between the quoted errors for the [Eu/H] values and the standard deviation of the resulting dispersions.

We find that the mean of the [Eu/H] errors acquired from the Delgado-Mena sample is $\sim$0.1 dex, which is important to note when comparing to our standard deviation of the residuals from our analysis. For our 2D detrended distributions, we see values slightly less than the quoted average error (Fe Tot: 0.074, Mg Tot: 0.087, Fe Thin: 0.064, Mg Thin: 0.084). Comparing the standard deviation (sigma) values to the errors allows us to determine if any of our outliers are real, which is to say that they exist in the data not due to analysis techniques but because of their own properties, i.e., intrinsic variation. The way we determine this is if our sigma value is greater than the average error in [Eu/H], we suspect that there are real outliers in the data.

The Fe detrending results in smaller sigma values than the Mg detrending. This suggests that the Fe abundance, with an average error of about 0.02 (dex), affects the [Eu/H] distribution more than the Mg abundance, which has an average error of 0.05 (dex). Where the Mg parameter consistently has greater errors than the Fe parameter, it is reasonable to assume that its resulting sigma values would be larger than Fe's sigma values. There is a small difference in the sigma values seen between the different populations, where the thin population distribution has a smaller value than the total population distribution. The likely cause of this is that the other populations have fewer data available in this dataset and are subject to more deviation as a result. This tells

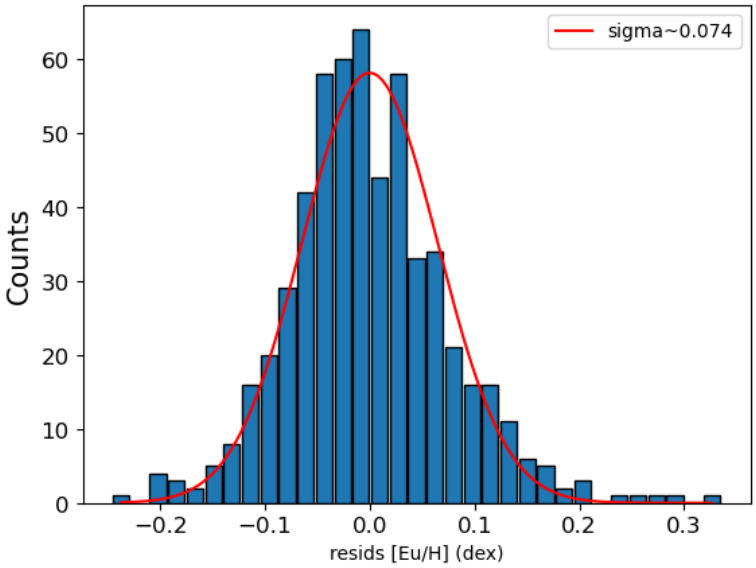

Figure 3.9: Histogram of the residual [Eu/H] in the total population after the 2D detrending according to [Fe/H] & Teff. The red line depicts a Gaussian best-fit line to the data.

us that we can better study the thin disk stars due to their prevalence in the data.

The results of our histogram distributions led us to inspect the observation errors of the abundances and compare them to the residual values. We show this in figure 3.13, where we look specifically at the Fe detrended [Eu/H] residuals, and we compare directly to the errors associated with each measurement. This effectively works as a 'σ' plot, where the y-axis is the σ level, which allows us to count the number of values in each region, telling us if any of the values are real outliers much like what comparing the standard deviations of the distribution to the average errors tells us. What this figure (3.13) shows is that there are 10 stars in the Delgado-Mena data that are very likely to be real outliers, as they exist above the 3σ range, which for a dataset this size is extremely unlikely as we would expect only 2 in this range.

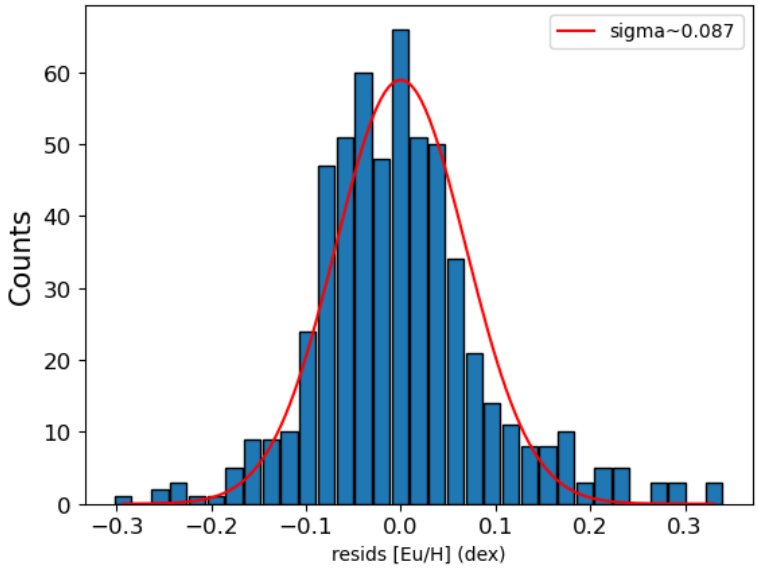

Figure 3.10: Histogram of the residual [Eu/H] in the total population after the 2D detrending according to [Mg/H] & Teff. The red line depicts a Gaussian best-fit line to the data.

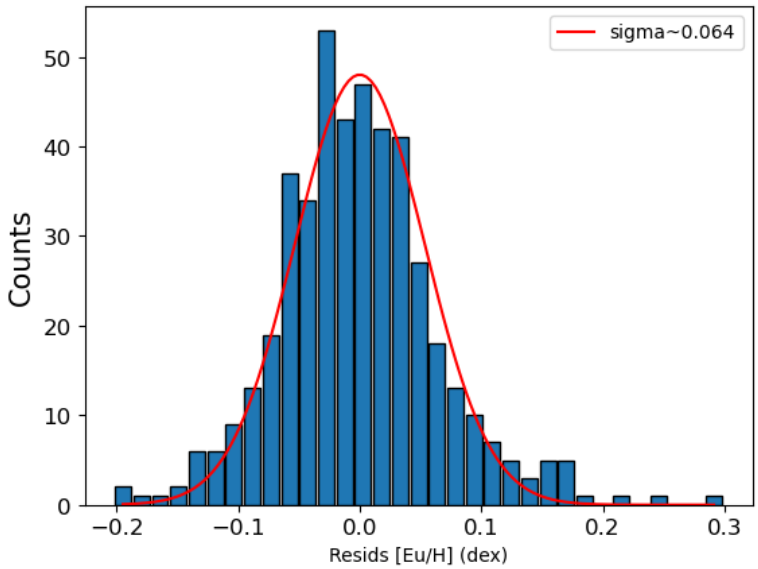

Figure 3.11: Histogram of the residual [Eu/H] in the thin population after the 2D detrending according to [Fe/H] & Teff. The red line depicts a Gaussian best-fit line to the data.

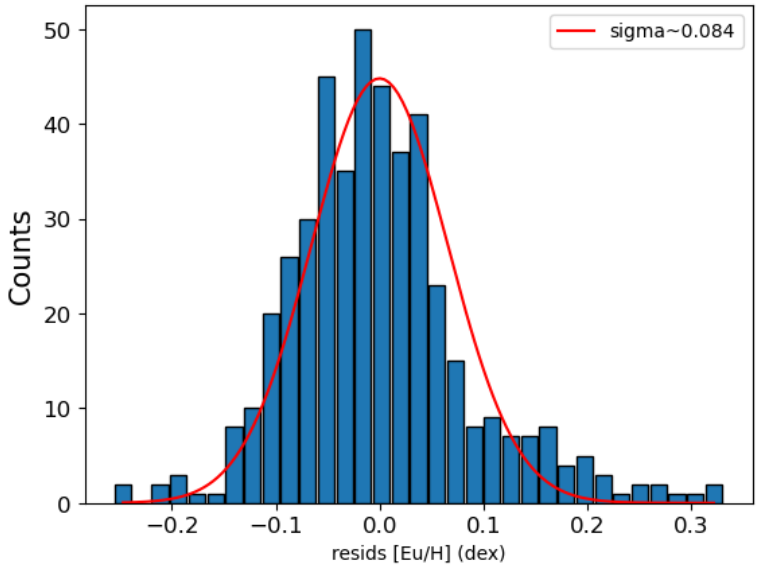

Figure 3.12: Histogram of the residual [Eu/H] in the thin population after the 2D detrending according to [Mg/H] & Teff. The red line depicts a Gaussian best-fit line to the data.

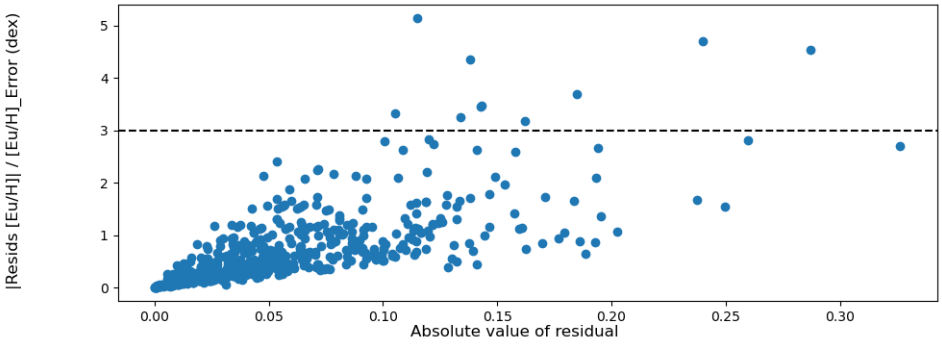

Figure 3.13: [Eu/H] residual values from the detrending process divided by the error compared to the error we divided by. This is for the Iron-based 2D detrending of the Delgado-Mena data.

What the analysis of the Delgado-Mena shows us is that Eu production works on similar timescales to both Fe and Mg, although they are created via different events. With this in mind, we do see that Fe tracks with age stronger than Mg does, which can be seen via the significant residual trend with respect to Age that the [Mg/H] detrending has compared to no significant residual trend from the [Fe/H] detrending. Another thing we found interesting, while peculiar, is that our analysis of the data results in [Eu/H] having a significant trend with Teff, which does not seem like a physical relationship and could be due to how the data is being looked at. In order to test if these takeaways are unique to this dataset, we explore these same trends in the dataset of B&B.

3.2 Battistini & Bensby

The results of our analysis of the Battistini & Bensby data allow us to compare the two datasets and what our models tell us about them. The B&B dataset is smaller than the Delgado-Mena dataset (566 stars) with a set of 378 Eu positive stars and does not differentiate between the different populations (i.e., thin, thick disk, halo and hαmr) the stars occupy.

We follow a similar pattern as seen for the Delgado-Mena data and convey the results in the same manner, where these graphs are simpler due to there being no population listings in the data.

In figure 3.14, we see a statistically significant negative slope that is similar in magnitude to what we see for Delgado-Mena. This indicates that the [Eu/H] abundance

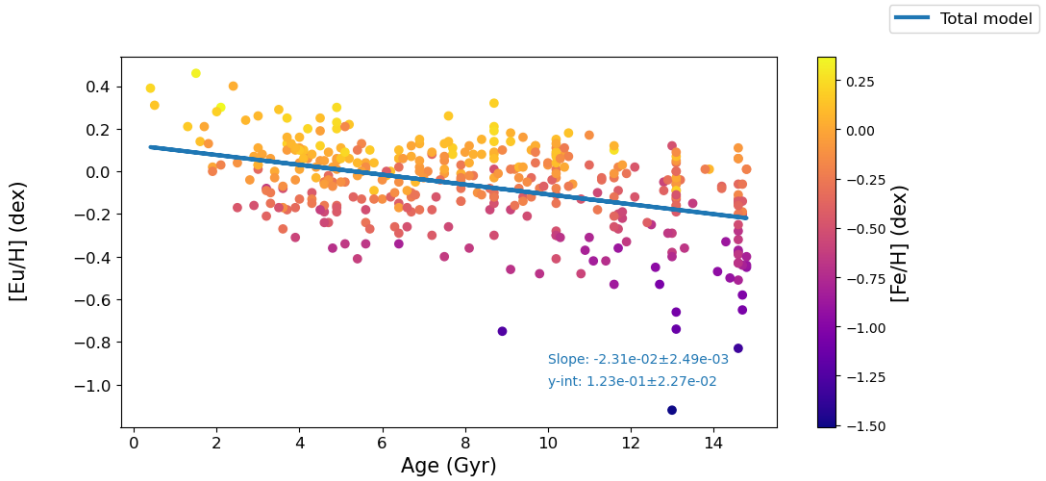

Figure 3.14: Raw [Eu/H] abundance as a function of Age with a [Fe/H] distribution bar. The resulting relationship conveys that there exists a similar correlation between [Eu/H] and Age that is seen in the Delgado-Mena dataset. The P-value for this plot is less than α, which tells us that it is an acceptable model.

of a star has some correlation to the age in that the relationship dictates a younger star is more likely to have more Eu. However, much like our analysis for the Delgado-Mena dataset, we aim to observe the effects of detrending select parameters on the variance of Eu, and comparing it to age allows us to develop our understanding of Eu in the context of galactic evolution. We also use the raw relationship with age as a baseline relationship that we will compare back to test if our detrending analysis has an effect on the confidence of the modeling procedure.

For fig 3.15, we see a positive correlation between residual Eu and Fe, much like in 3.2. There is a slight discrepancy in the value of the slopes, where the errors on each don't cause these values to overlap. The slope from the Delgado-Mena sample is slightly larger for the total population and even more for the thin population. The importance of this is that this positive correlation is of similar magnitude, which leads us to expect

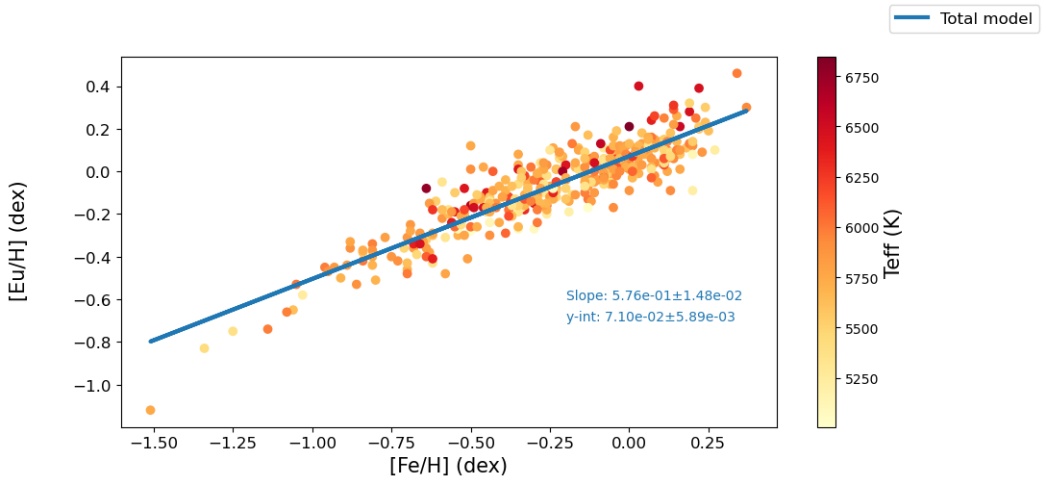

Figure 3.15: [Eu/H] vs [Fe/H] with Effective Temperature as the color distribution. A positive correlation is seen from the blue best-fit line. The P-value for this plot is less than α; this tells us it is an acceptable model.

a similar relationship in the rest of the galaxy. This allows us to continue our analysis of the data to see if there are any significant differences we see when comparing back to the Delgado-Mena analysis.

We see in fig 3.16 a positive correlation between residual Eu and Teff that happens to be marginally statistically significant. This is contradictory to what we see in fig 3.3, which portrays a negative correlation of nearly the same magnitude. This revelation brings up questions that we will discuss further in the discussion section.

For fig 3.17, we see a positive slope between residual Eu and Age that is almost identical to the slope seen in fig 3.4 total model (blue) with the respective values being $2.32 * 10^{-3}$ for B&B and $2.35 * 10^{-3}$ for Delgado-Mena. This is interesting even when considering the models are not statistically significant and that our analysis results in very similar values for the relationship. The errors on the model slopes differ slightly,

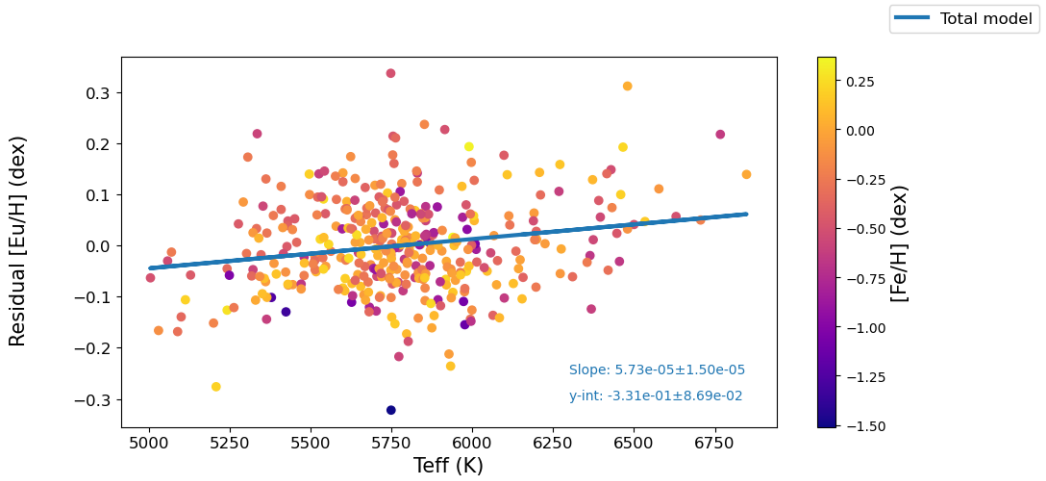

Figure 3.16: [Fe/H] Detrended from [Eu/H] vs Effective Temperature. A positive correlation is shown by the blue best-fit line. The P-value for this plot is the closest to α but is still less than α; this tells us it is an acceptable model, however only marginally so.

which is likely due to the errors associated with initially calculating all the related parameters to this analysis. The sample size of Delgado-Mena is larger, allowing a more robust approximation than when compared to the B&B data, as seen by the smaller errors associated with the respective resulting slopes. We speculate the cause of the statistical insignificance, as stated previously, to be rooted in the fact that since Eu and Fe track together at similar rates when we eliminate the Fe trend from the data, we are losing statistical weight.

Now that we have categorized what happens to [Eu/H] when we look at its relationship with [Fe/H] and how that relationship affects [Eu/H]'s other relationships, we can move to the [Mg/H] relationship to compare back to our Delgado-Mena analysis.

Much like before, we show the [Eu/H] abundance relationship with age in fig 3.18. We see that the [Mg/H] acts like the [Fe/H], which we show in more detail in fig

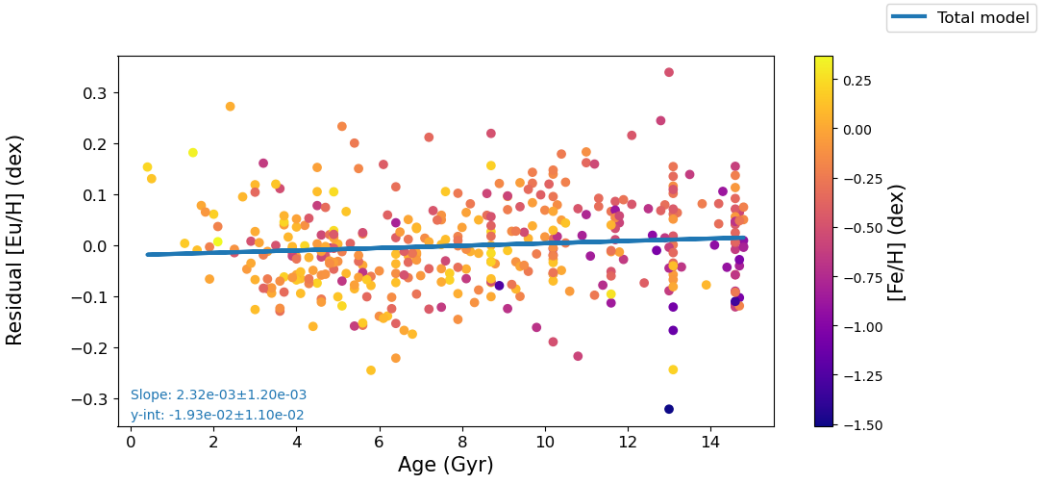

Figure 3.17: [Fe/H] & T_{eff} detrended from [Eu/H] vs Age. Similar to Figure 3.4 for the total model(blue), a positive correlation can be seen. The P-value for this plot is also greater than α, which tells us that it is not an acceptable model.

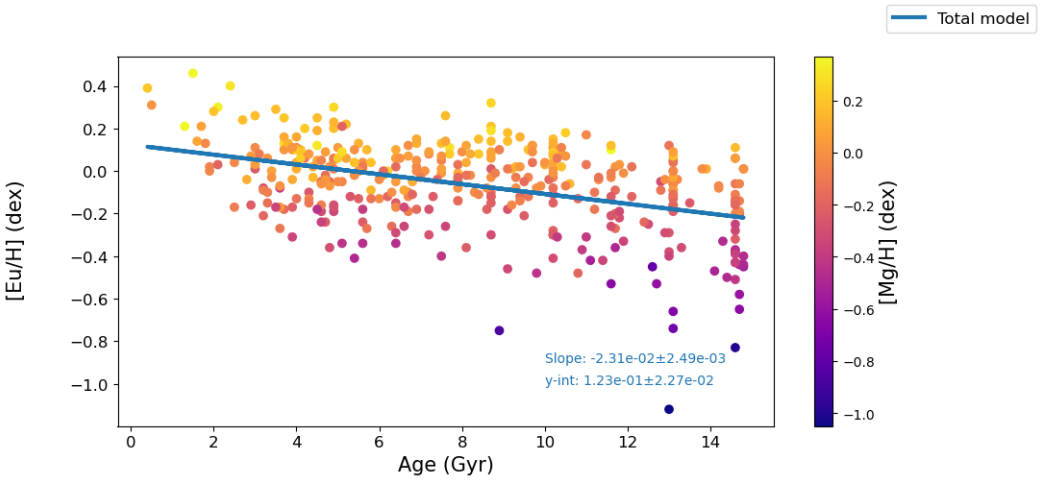

Figure 3.18: Raw [Eu/H] vs Age with a [Mg/H] distribution color bar. The only difference in this plot when compared to Figure 3.14 is the color distribution. The P-value for this plot is less than α, which tells us that it is an acceptable model.

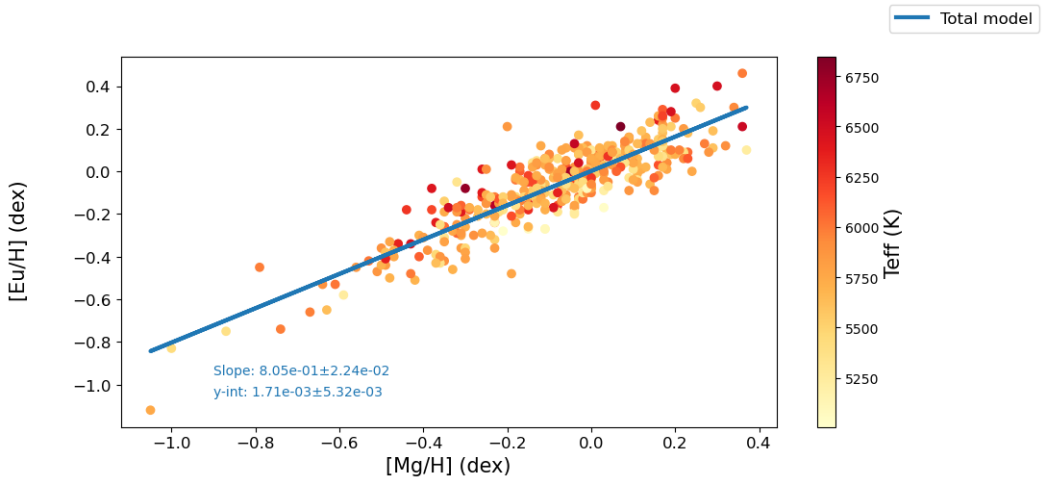

Figure 3.19: [Eu/H] vs [Mg/H] with an Effective Temperature color distribution. The best-fit line corresponds to a positive correlation in the relationship of the two abundances. The P-value for this plot is less than α; this tells us it is an acceptable model.

3.19.

Similar to what we saw for the figures 3.15 and 3.2 that describe the relationship of [Eu/H] with [Fe/H], we see the same for figures 3.19 and 3.6 that describe the relationship of [Eu/H] with [Mg/H] instead. Where there is a difference in quoted slope values between the two datasets, in the case of abundance relationships, it happens to be a little more prominent for the Fe models when compared to the Mg models. It is important to note that the errors in the slopes of the total model from Delgado-Mena and the model from B&B are less than the difference of the slopes, meaning they do not encompass the other slope value within their own range of possible slope values. Although these aspects are important factors to account for, this figure does create confidence in the idea that Mg tracks with Eu on a similar timescale to that of Fe.

For fig 3.20 we again see a positive correlation between the residual Eu and

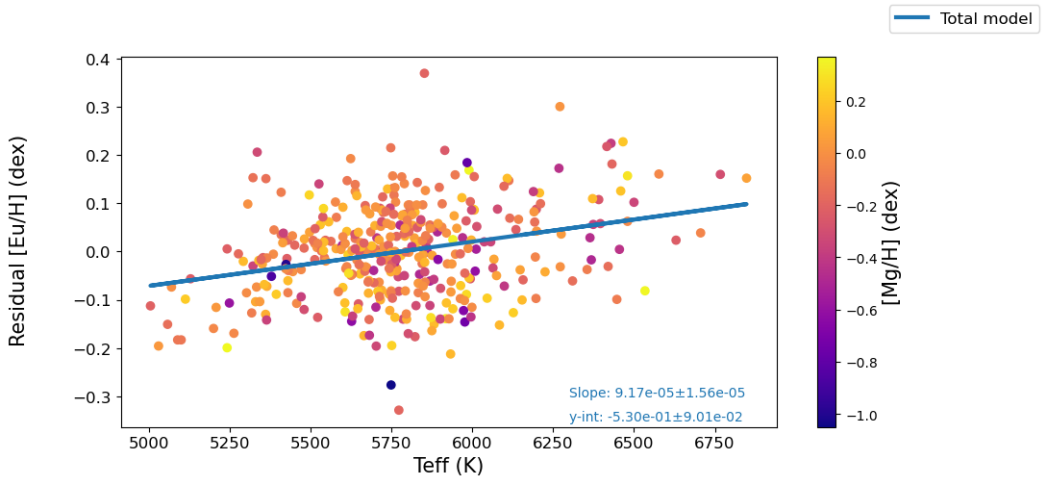

Figure 3.20: [Mg/H] Detrended from [Eu/H] vs Effective Temperature. A positive correlation can be seen via the best-fit line in blue. The P-value for this plot is less than α, which tells us that it is an acceptable model.

Teff as seen in 3.16, which contradicts what we saw for the Delgado-Mena dataset in figs 3.3 and 3.7. This is a statistically significant relationship as seen in the other figures 3.3, 3.7, and 3.16, each describing a similar analysis resulting in slopes of similar magnitude but in different directions is inherently quite puzzling. We further discuss this puzzling nature in the next chapter to finish our analysis of the B&B data in the same manner as we did for the Delgado-Mena data.

Our detrending analysis has brought us back to the relationship [Eu/H] has with age, and we show this final version of the relationship in fig 3.21. What we see is a negative correlation that is not statistically significant, contrary to both of the other relationships [Eu/H] has shown with age in the Battistini and Bensby data, as displayed in figs 3.14/3.18(these two figures are the same physically and only differ due to the color distribution explaining the different element abundances) and 3.17. This

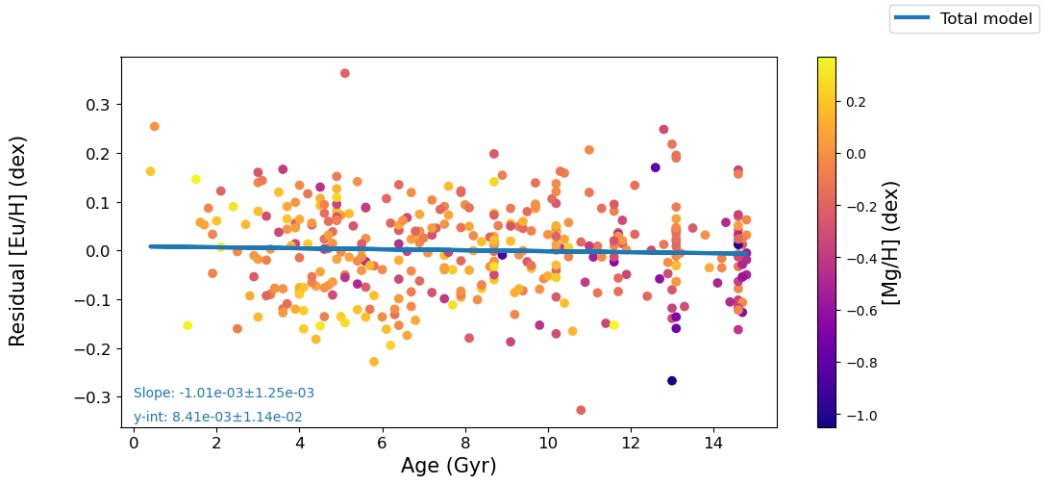

Figure 3.21: [Mg/H] & T_{eff} detrended from [Eu/H]. A negative correlation is seen by the best-fit line. The P-value for this plot is greater than α, this tells us it is not an acceptable model.

negative correlation is in line with what we saw in the Delgado-Mena data; however, the magnitude of the relationship seen in 3.21 ($-1.01 * 10^{-3}$) is a factor of almost exactly ten less than the one seen for the total model of the Delgado-Mena data in fig 3.8 ($-1.08 * 10^{-2}$). It is, however, important to note this relationship seen in fig 3.21 is not significant; thus, scrutinizing it too deeply is detrimental to our argument. This dataset has created a few questions for us to examine, and we finish off the analysis by plotting the distributions of the [Eu/H] abundances before and after our analysis to better prepare our attempt to explain some possible solutions to these questions.

The raw abundance distribution for the B&B data is shown in fig 1.4, which is near the end of the introduction section. From this distribution, we see a non-normal distribution that has a few outliers. If we compare our sigma value (0.202) to the error quoted for [Eu/H] (0.08), we find that our sigma value is larger than the quoted error

by roughly a factor of 2.5 which we suspect is due to the Metallicity term, and to a lesser extent the Teff term adding systematics to the relationship. Without performing our detrending analysis, a result like this would tell us that there is significant variation in [Eu/H] values; however, if we take into account the inflationary terms by detrending them, they change the sigma value from 0.202 to ∼0.09 (average of 0.088 & 0.092). Doing this changes the intensity of the variation we are looking for.

Comparing the raw data histograms from both datasets (figs 1.3 and 1.4), we see that their sigma values are close to one another, with much of the data existing in the same region, where for the B&B data there exists some outliers on the negative end. This observation can be paired with the fact that the B&B data has a slightly higher percent of (Eu) metal-poor stars, with about 57% of the stars having [Eu/H] less than 0 compared to Delgado-Mena's 54% of stars with [Eu/H] less than 0. Knowing that the datasets have similar distribution properties before our analysis leads us to suspect that they will have similar properties after our analysis.

For figures 3.22 and 3.23 we see the resulting distributions of the [Eu/H] values after our detrending analysis. They are non-normal distributions with smaller sigma values than what we saw for the raw abundance distribution seen in fig 1.4. Like what we saw for the Delgado-Mena dataset, the peak-to-peak values are more constrained for both versions of the detrending, where the sigma value for the Mg detrending is greater than the sigma value corresponding to the Fe detrending. This data seems to have a few outstanding outliers by the looks of the initial distribution, which is reduced to a similar level of the Delgado-Mena data after our analysis; however, the Mg detrending

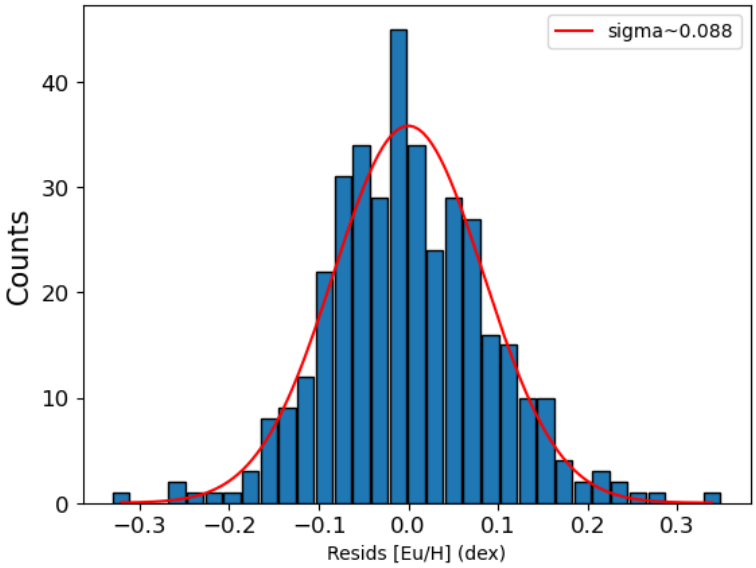

Figure 3.22: Histogram distribution of the Dual factor ([Fe/H] & Teff) Detrended [Eu/H]. The red line represents the best-fit Gaussian

seems less effective at reigning in the outliers, which results in a larger overall peak to peak distribution as well as a larger dispersion (sigma). This is likely due to the Mg abundance values having larger associated errors than the Fe abundance values. We also note that the sigma values for the B&B dataset are greater than the sigma values seen for the Delgado-Mena data.

Figure 3.24 shows the comparison of the [Eu/H] values to the single-quoted error for the Battistini and Bensby data of 0.08 dex, which is why it results in a line of points. Much like in figure 3.13, this plot acts as a 'σ' plot where for this dataset, we see 5 stars above the 3σ level where we would expect one star around this level for the sample size. We choose to show the [Mg/H] version of the detrending for the B&B dataset as compared to the figure we show for the Delgado-Mena data (fig 3.13),

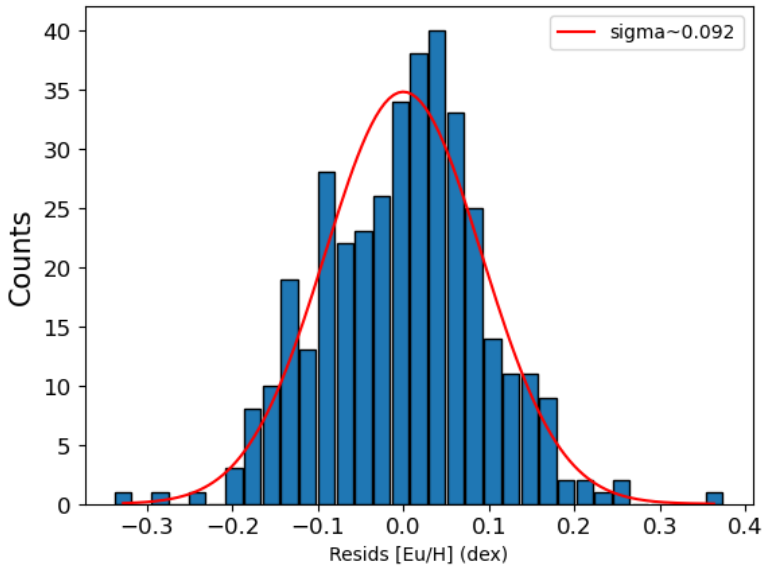

Figure 3.23: Histogram distribution of the Dual factor ([Mg/H] & Teff) Detrended [Eu/H] values for the B&B data. The red line represents the best-fit Gaussian

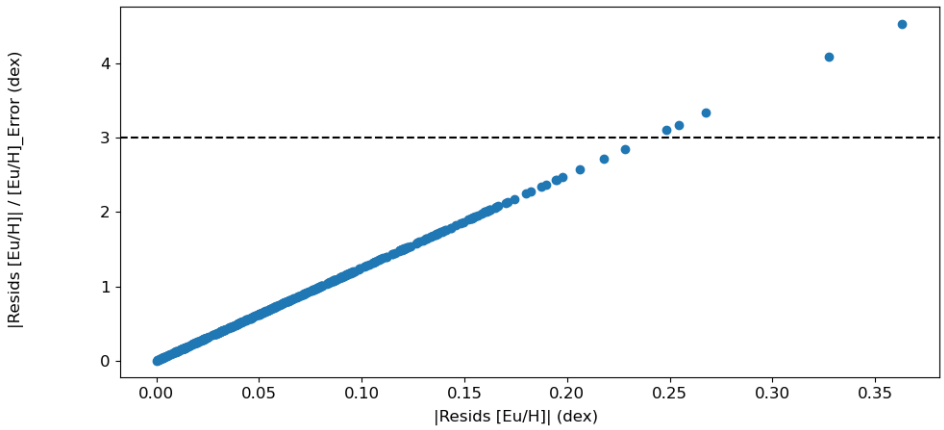

Figure 3.24: Absolute value of the [Mg/H] Detrended [Eu/H] residuals divided by the Error in [Eu/H] measurements compared to the Absolute value of the Detrended [Eu/H] residuals. It is represented as a straight line of points due to the singular error value from the source material

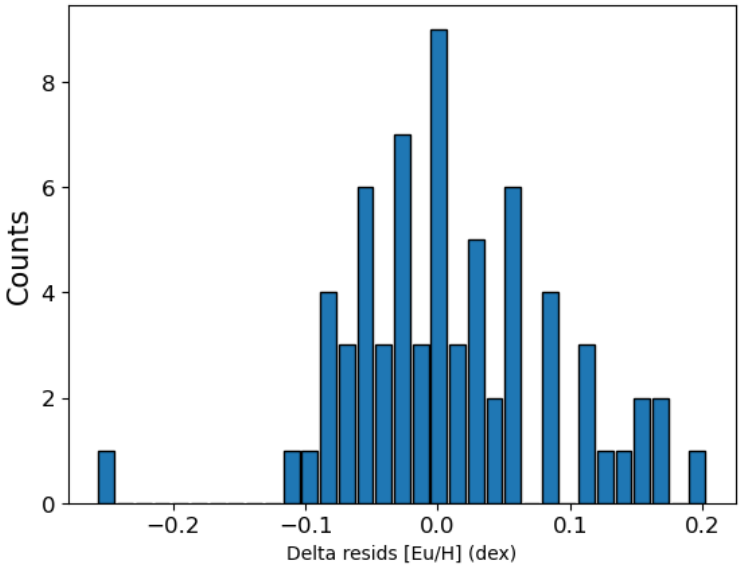

Figure 3.25: Histogram distribution of the difference (Delgado-Mena-B&B) in detrended [Eu/H] values of the overlapping data within each dataset. The average value of the distribution is ∼0.06 dex, where the standard deviation is ∼0.075 dex.

which was detrended by [Fe/H]. The reason for this choice is the idea that we wanted to look at the more interesting parameter from either dataset, whereas, for the Delgado-Mena dataset, it was the Fe parameter strictly due to the insignificance of the model in fig 3.4. Whereas, for the B&B dataset, both metallicity parameters resulted in insignificant models for the 2D detrended relationships with respect to Age, so instead, we chose to look at Mg due to it being another interesting parameter, where showing both parameters effects for both datasets in this manner would be redundant due to the histogram plots we show assisting us.

3.3 Shared Sample

We found that there are 68 stars in common between the Delgado-Mena and Battistini & Bensby datasets. A comparison of the difference in the [Eu/H] abundances is shown in Figure 3.25. The standard deviation of the resulting distribution results in a value of 0.075, which is comparable to what we see in the other histograms we present for both datasets after we detrend (figs 3.9, 3.10, 3.11, 3.12, 3.22, 3.23). We expect that this sigma should be the size of the errors in Delgado-Mena and Battistini and Bensby added in quadrature. The typical error for [Eu/H] quoted in Battistini and Bensby is 0.08, and Delgado-Mena is 0.1, which, when added in quadrature, is roughly 0.13, which is significantly different than our sigma value for the combined distribution seen in fig 3.25.

Since the sigma value is not the same as the quadratic sum in this case, it leads us to suspect that Delgado-Mena and B&B are overestimating their errors. The Delgado-Mena team calculates their errors for Eu abundances using MOOG, considering Hyperfine Splitting (HFS) for the abundance value using a method that looks at the Equivalent Widths (EW's) [10], which uses the Full Width Half Max (FWHM) of the spectral lines from ARES. This method accounts for calculated uncertainty such that the statistical photometric error due to the noise in each pixel and the error related to the continuum placement, which is the dominant contribution to the error. Their error analysis also takes into account the stellar parameter error propagation for the Teff, log(g), and microturbulence ξ, each with varying degrees of effect on the error

associated with the abundances they find.

As for the B&B team, they acquire their abundance values using Spectroscopy Made Easy(SME) to create synthetic spectra to use in their comparison with the observed spectra. For this, they use a minimization routine of an unnormalized χ^2 function based on the difference between the observed and the synthetic spectra. They estimate the random errors by deriving how much the errors of the stellar parameters Teff, log(g), and ξ (which are also used in Delgado-Mena) would affect the final abundances. Using this method, they calculated the difference between the abundances with and without the errors on stellar parameters applied, then all the differences for each element were used to calculate the final square mean error, resulting in a singular error for the respective elements.

Much like the case for [Eu/H], we compare the average errors of these parameters to the standard deviation of the differences (DM-BB) between the two datasets for the stars that happen to be in both datasets. What we find is that for Teff, the quadratic sum of the mean error values, 21K for Delgado-Mena, and 63K for B&B, results in 67K, whereas the standard deviation of the differences in the Teff for the overlapping sample is 43K. Similarly, for the other parameters, we find that each of them shows the same result. Thus, the two analyses are better at determining the stellar parameters than their adopted errors suggest. This is evidence that there is an overestimation of errors that, as a result, inflates the errors of the Eu abundances, which negatively affects the search for intrinsic variations.

Chapter 4

Discussion

The importance of this study is that it is meant to attempt to determine the abundance variation of [Eu/H] for the future work of modeling terrestrial planet geothermal behaviors. We do this by critically examining the correlations found with Fe, Mg, Teff, and age to Eu in an effort to constrain our understanding of the star-to-star variations of the Eu abundances as well as to determine the magnitude of the variations. Knowing the amount in which [Eu/H] varies allows us to constrain the thermal evolution models that depend on the abundances of radiogenic elements as well as silicates. Constraining thermal evolution models allows us to better determine the likelihood of an exoplanet being geologically active in a similar manner to Earth, which, as we discussed in the introduction, is an important factor for the evolution and longevity of life.

Our linear fits of the data allow us to understand the correlation of the respective parameters compared to the [Eu/H] abundance. These trend lines are used in

the detrending analysis that we perform to determine the [Eu/H] abundance variation. In our results section, we explain the apparent outcomes for the respective figures in that section, whereas, in this section, we aim to discuss the overall implications of our findings. In order to be concise, we will compare the findings for both Delgado-Mena and B&B simultaneously, looking at the similarities and the differences for the figures that share the same format (i.e. [Eu/H] vs. Age, [Eu/H] vs. [(Fe or Mg)/H], 1D(Fe or Mg) detrended [Eu/H] vs. Teff, and 2D detrended [Eu/H] vs. Age) where we end the discussion with the comparison of the same stars within the datasets, following the general order of the figures depicted within the results subsections.

When we compare the results from the separate datasets, it is important to note that we compare the 'Total model'(the line/values in blue) from the Delgado-Mena data to the data in B&B. As an overall note in the Delgado-Mena data, the internal comparison of the 'Thin model'(the line/values in red) to the 'Total model' is meant to convey an example of how taking the galactic population into account can alter the trend observed, in which, many instances we find little difference between the thin and total model trends. Wherein the unique incidents of a more significant difference being observed, further elaboration will be noted for that particular figure.

Starting with the Raw abundance trends with Age seen in figures 3.1, 3.5, 3.14 and 3.18, we note that what we observe is to be expected, as the abundances are higher for younger stars when compared to lower concentrations for older stars [17, 19]. This is an example of chemical enrichment which describes that over the lifetime of the universe, heavier elements become more prevalent which are bound to be an ingredient in stellar

objects such as stars, planets, gas clouds, etc. These plots also convey the relationship Fe has with the [Eu/H] and Age parameters, where it is observed in a similar fashion that Fe concentrations go up for younger stars which again is explained with the idea of chemical enrichment. However, we show the relationship that [Eu/H] has with [Fe/H] and [Mg/H] in more detail in the figures 3.2, 3.6, 3.15, and 3.19 to better understand their correlation to one another.

For the relationship between [Eu/H] and [Fe/H] (fig 3.2), we observe that for the Delgado-Mena data, the trend lines for the thin and total data show a visible difference in slope values. What we take away from this relationship is that for sufficiently sized datasets, it is important to differentiate the stellar populations as it could have an overarching effect on the analysis moving forward. Similarly, if we compare the total model trend from Delgado-Mena to the B&B trend (fig 3.15), what we see is a difference of similar magnitude to what we saw for the internal comparison in Delgado-Mena's populations. Each of the trend lines gives us the information that [Eu/H] and [Fe/H] track with one another; however, not exactly at a 1:1 ratio. This result is expected considering the sources of the respective elements are likely different, and each population may have different metallicity dependencies [19, 17, 28].

Looking at the relationship that [Eu/H] has with [Mg/H] (figs 3.6, 3.19), we see similar trends with less variability than is seen in the [Fe/H] relationship. When observing the trends for the [Fe/H] and [Mg/H] analyses side-by-side, we see a different pattern in how the magnitudes of the slopes act when looking at the plots in the order: DM thin, DM total, BB total. Following this order, for the [Fe/H] analysis, we see

that the slope magnitudes decrease, whereas for the [Mg/H] analysis, we see the slope magnitudes increase. This signifies that [Fe/H] and [Mg/H] behave differently when accounting for all the populations, where their thin disk behavior is nearly identical, which can be seen by the similar slopes in the Delgado-Mena thin trends seen in figures 3.2 (0.752 ± 0.0164) and 3.6 (0.751 ± 0.0236). The [Mg/H] results allow us to come to a similar conclusion we came to with the [Fe/H] trends, which is that [Mg/H] tracks with [Eu/H] albeit not at a 1:1 ratio and that it does not track as strongly as [Fe/H].

The largest discrepancies between the two datasets are displayed in the figures concerning the relationship between the 1D-detrended [Eu/H] and Teff (figs 3.3, 3.7, 3.16, 3.20) as the relationships from Delgado-Mena show a negative correlation and the B&B show a positive correlation. This is the case for both instances of detrending either the [Fe/H] or [Mg/H] contributions from the [Eu/H] values. This is interesting for two reasons, the first being that we do not expect a strong trend between these two parameters, as the Teff of stars with a common origin often has no bearing on element abundance [27]. The second reason is that these two independent studies found conflicting information, which is a signal that there is something in their respective analyses causing this discrepancy. What this tells us is that moving forward, due to the systematics we show, we should perform a detrending analysis that accounts for these systematics, as there should not be a correlation between Eu and Teff.

For the 2D detrended [Eu/H] vs. Age plots (figs 3.4, 3.8, 3.17, 3.21), in the case of Delgado-Mena, there is a visible distinction of the trends for both versions of the 2D detrend (i.e., Teff and Fe or Mg). However, the only plot in this subset that

we can look at and scrutinize the slope differences is fig 3.8, as this is the only plot with significant trends. The other three figures (3.4, 3.17, 3.21) do not have significant trend lines. Another takeaway from the Fe detrending is that most of [Eu/H]'s age correlation is eliminated in this process which tells us that attempting to determine [Eu/H] variation with age is not very effective, as there is a likelihood that the [Eu/H] vs. age relationship is dominated by the [Fe/H] factor. With this takeaway in mind, we find that both metallicity terms ([Fe/H], [Mg/H]) impact the [Eu/H] abundance more than the Teff and Age parameters which is why we choose to focus on the Metallicity detrended plots versus a version where we detrended by Teff or Age alone.

As for the Mg version of the 2D detrending of [Eu/H] vs. Age (figs 3.8, 3.21), we see that the two datasets have differing results when compared to one another. There is a slight difference in the thin model trend slope and total model trend slope for the Delgado-Mena dataset, with a more significant difference seen between the total model trend slopes between Delgado-Mena and B&B. The fact that the trend lines differ significantly from one another in fig 3.8 tells us that [Mg/H] in the thin disc acts differently when compared to the other stellar populations. The difference we see in the Delgado-Mena sample could be due to the heavy concentration of old stars with a relatively high residual of [Eu/H]. The Delgado-Mena plot (3.8) has statistically significant trends, which is not seen in the B&B plot (fig 3.21); the reason this is the case perhaps comes down to sample size and the sample population density ratios. We do show an insignificant slope for figure 3.21, which would imply a similar finding to our [Fe/H] case in relation to how it affects [Eu/H]'s relationship with age. However, since

we see differing results between the two datasets, we come to the conclusion the Mg contribution to the [Eu/H] vs. Age relationship is minimal, unlike the Fe contribution, which reinforces the idea that [Fe /H] dominates the [Eu/H] vs. age trend.

Many correlations we show via our trend lines are significant (Table A.1). We note that the 2D detrending with respect to [Fe/H] results in insignificant trends across the board, where we see conflicting results for the [Mg/H] detrending. The Delgado-Mena sample results in significant trend lines after decorrelating [Mg/H] and Teff from [Eu/H] (fig 3.8), which contradicts the B&B result of an insignificant trend line in fig 3.21. A critical difference between these two figures is that the sample size is different and may contain different stellar population ratios, which is likely the driving factor in the contradicting results.

Our histograms (figs 3.9, 3.11, 3.10, 3.12, 3.22, 3.23) are an attempt to understand the peak-to-peak distribution as well as the standard deviation of the residual [Eu/H] values. We find the peak-to-peak ranges for each of the variations in both datasets are close to one another, including the comparison between the two separate datasets. The variation in results comes from the differences in the standard deviation values (sigma as noted in the figures) where the B&B dataset has outliers of larger magnitude which is a driving factor for these differences. Alongside the histograms, we show our σ plot, which tells us how many stars have a [Eu/H] value within a reasonable range. We find that there is a higher amount of stars that exist in high sigma ranges than expected from the sample sizes, which is evidence of true outliers.

For the 68 shared stars, we note that the two teams used different methods to

acquire their [Eu/H] values, which causes the measurements to differ in the respective datasets. As seen in figure 3.25, the average difference in the detrended [Eu/H] values is non-zero with a standard deviation value on par with the other values we acquired, telling us that the different methods used result in significantly different values which is why it poses a problem. The differences in the measurements from the respective datasets could originate from the fact that both analyses show evidence of overestimating. The magnitude of the overestimation could vary from star to star for both analysis methods, and each can be heavily influenced by the systematic variances we show arising from Metallicity, Teff, and Age.

Tying things back to the motivation for this project, for Figure 1.2 from Nimmo [23], we explain that variations in radiogenic abundance can have significant consequences for the thermodynamic evolution of a terrestrial planet's interior. We then introduce equation 2.9 in our Equations subsection as a method to compare our results more directly with this motivating figure. Taking an average of the slopes from Delgado-Mena (0.818) and B&B (0.812) results in 0.815 which, when used in equation 2.9 results in the Mg term looking like $-0.185 \cdot [Mg/H]$. From this, we note that the [Mg/H]'s peak-to-peak ranges from -0.5 to 0.3 dex, which would tell us that on Fig 1.2, we would move up and down about 0.09 and -0.06 dex. Accounting for the $[\text{Eu/H}]_{res}$ term, we use the average of the sigmas quoted in figures 3.8 (0.087) and 3.21 (0.092) we get 0.09, whereupon adopting our 3σ significance to cover 99.7% of the population, we see an up and down shift of ± 0.27 dex on top of the metallicity shift.

Chapter 5

Conclusion

For this project, we have analyzed data from a few different papers [3, 5, 11, 12], where the two documents from the Delgado-Mena team share a dataset, and the Battistini & Bensby paper shares a dataset with the Bensby paper. We analyze the data from the respective teams to search for intrinsic variation in Eu abundances. We search for the intrinsic variation in Eu abundances for the purpose of better constraining geothermal evolution models as detailed by Nimmo in [23]. We do this by comparing the trend lines of [Eu/H] to Age and a metallicity parameter that takes either [Fe/H] or [Mg/H] as the argument. After this comparison, we detrend either metallicity term from the [Eu/H] values and then compare it to Teff. After comparing to Teff, we detrend this relationship in a similar manner as the metallicity term to compare back to the Age parameter. What we find from these trend lines is that there exists a significant correlation between many of these parameters and [Eu/H]. However, for the residual trend lines for the 2D detrending, the statistical significance varies for the relationships

we look at. Specifically, the relationship residual [Eu/H] has with Age and [Mg/H] is the subject of this variation in significance.

Similarly, we learn that there is an odd relationship seen between the 1D residual [Eu/H] (1D-detrended by [Fe/H] or [Mg/H]) and Teff, such that the results from the two datasets contradict one another for both metallicity parameters, where the Delgado-Mena dataset has a positive correlation, and the B&B a negative correlation. While describing this contradiction, we also note that the trends that the now detrended [Eu/H] values have with Teff are uncharacteristically strong. Noting that for the 68 stars that are shared between the two datasets, the differences seen in quoted Teff values range from around -100K to 130K, which could in part help describe this contradiction, it does not, however, explain why the relationship is as strong as it is. These trends of [Eu/H] against Teff for both datasets are near equal to each other in terms of magnitude but of opposite signs, which poses a thought-provoking question; why has this not been accounted for more widely in the scientific community? Although we argue for caution when using Teff as a useful parameter in searching for the intrinsic variation due to these relatively strong but conflicting relationships, we find that the impact observed on the [Eu/H] values is less than the impact observed for the metallicity parameter cases.

The metallicity parameters are seen to have the largest effect on [Eu/H] abundances, where the effect of age is similar to that of Teff, in which the overall change in variation of Eu is minimal. These parameters are not the only parameters that could inflate any associated error in [Eu/H], but they are the ones we chose to look at due to the prevalence they hold in large searches as well as the importance they share in

searching for Earth-like exoplanets and modeling geological activity for terrestrial planets. Other parameters, such as the log(g) and ξ, are used in the process of acquiring the Eu abundance values, which is another source of the inflation in errors associated with abundance measurements. It is possible that there are other parameters that share a non-trivial link to artificially inflating abundance variations; however, from our analysis, we show that the Metallicity, Teff, and Age parameters contribute to this inflation which should be accounted for if performing a similar search for abundance variations. We find that an average standard deviation of the distributions results in a 'sigma = 0.085,' which is slightly greater than B&B's estimated error for [Eu/H](0.08) and less than the average error in the Delgado-Mena data (0.1). Taking our variation to be 0.085 dex, we expect the peak-to-peak values for the [Eu/H] abundance to be around $\pm$0.26 dex. This analysis finds little evidence of significant intrinsic variation of Eu in a star-to-star capacity, with a few exceptions that stand out as outliers in the distributions. The datasets have an average outlier rate of about 1.5%, with the most extreme outliers being around the 5σ level corresponding to an average residual [Eu/H] value in dex of about 0.17 for Delgado-Mena and 0.29 for B&B which, when averaged together we get about 0.23 dex. (Delgado-Mena's Average residual [Eu/H] value for the outliers is within the peak-to-peak range for the primary reason that for their dataset, there exist associated errors with individual stars which means a smaller measured value can have an extremely small associated error which would constitute an outlier by our notation.)

The size of the errors for the data is likely inflated from a variety of sources, and due to this, we are unable to discern if what we see is a systematic variation. Future

analysis could look at an increased sample size of stars with similar or better resolution from specified locations in the galaxy to better model the respective locations so that we can better our understanding of galactochemical evolution. While minding the sources of error inflation, we expect that with a small enough error, it may allow us to observe with more certainty true star-to-star variation; however, it is likely small in magnitude due to what our analysis finds.

Bibliography

[1] V. Zh. Adibekyan, N. C. Santos, S. G. Sousa, and G. Israelian. A new α-enhanced super-solar metallicity population. , 535:L11, November 2011.

[2] Melike Afşar, Christopher Sneden, Anna Frebel, Hwihyun Kim, Gregory N. Mace, Kyle F. Kaplan, Hye-In Lee, Heeyoung Oh, Jae Sok Oh, Soojong Pak, Chan Park, Michael D. Pavel, In-Soo Yuk, and Daniel T. Jaffe. The Chemical Compositions of Very Metal-poor Stars HD 122563 and HD 140283: A View from the Infrared. , 819(2):103, March 2016.

[3] Chiara Battistini and Thomas Bensby. The origin and evolution of r- and s-process elements in the Milky Way stellar disk. , 586:A49, February 2016.

[4] Megan Bedell, Jacob L. Bean, Jorge Meléndez, Lorenzo Spina, Ivan Ramírez, Martin Asplund, Alan Alves-Brito, Leonardo dos Santos, Stefan Dreizler, David Yong, TalaWanda Monroe, and Luca Casagrande. The Chemical Homogeneity of Sun-like Stars in the Solar Neighborhood. , 865(1):68, September 2018.

[5] T. Bensby, S. Feltzing, and M. S. Oey. Exploring the Milky Way stellar disk.

A detailed elemental abundance study of 714 F and G dwarf stars in the solar neighbourhood. , 562:A71, February 2014.

[6] J. C. Bond, D. S. Lauretta, C. G. Tinney, R. P. Butler, G. W. Marcy, H. R. A. Jones, B. D. Carter, S. J. O'Toole, and J. Bailey. Beyond the Iron Peak: r- and s-Process Elemental Abundances in Stars with Planets. , 682(2):1234–1247, August 2008.

[7] R. B. Botelho, A. de C. Milone, J. Meléndez, M. Bedell, L. Spina, M. Asplund, L. dos Santos, J. L. Bean, I. Ramírez, D. Yong, S. Dreizler, A. Alves-Brito, and J. Yana Galarza. Thorium in solar twins: implications for habitability in rocky planets. , 482(2):1690–1700, January 2019.

[8] John M. Brewer and Debra A. Fischer. Spectral Properties of Cool Stars: Extended Abundance Analysis of Kepler Objects of Interest. , 237(2):38, August 2018.

[9] Aarynn L. Carter, Sasha Hinkley, Mariangela Bonavita, Mark W. Phillips, Julien H. Girard, Marshall Perrin, Laurent Pueyo, Arthur Vigan, Jonathan Gagné, and Andrew J. I. Skemer. Direct imaging of sub-Jupiter mass exoplanets with James Webb Space Telescope coronagraphy. , 501(2):1999–2016, February 2021.

[10] R. Cayrel. Data Analysis. In G. Cayrel de Strobel and Monique Spite, editors, *The Impact of Very High S/N Spectroscopy on Stellar Physics*, volume 132, page 345, January 1988.

[11] E. Delgado Mena, A. Moya, V. Adibekyan, M. Tsantaki, J. I. González Hernández,

G. Israelian, G. R. Davies, W. J. Chaplin, S. G. Sousa, A. C. S. Ferreira, and N. C. Santos. Abundance to age ratios in the HARPS-GTO sample with Gaia DR2. Chemical clocks for a range of [Fe/H]. , 624:A78, April 2019.

[12] E. Delgado Mena, M. Tsantaki, V. Zh. Adibekyan, S. G. Sousa, N. C. Santos, J. I. González Hernández, and G. Israelian. Chemical abundances of 1111 FGK stars from the HARPS GTO planet search program. II. Cu, Zn, Sr, Y, Zr, Ba, Ce, Nd, and Eu. , 606:A94, October 2017.

[13] Emily Griffith, Jennifer A. Johnson, and David H. Weinberg. Abundance Ratios in GALAH DR2 and Their Implications for Nucleosynthesis. , 886(2):84, December 2019.

[14] A. Kramida, Yu. Ralchenko, J. Reader, and and NIST ASD Team. NIST Atomic Spectra Database (ver. 5.10), [Online]. Available: `https://physics.nist.gov/asd` [2023, March 28]. National Institute of Standards and Technology, Gaithersburg, MD., 2022.

[15] Jessica Libby-Roberts. Observational Perspective on Linking Sub-Neptune Atmospheric Measurements to Planet Formation. In *American Astronomical Society Meeting Abstracts*, volume 54 of *American Astronomical Society Meeting Abstracts*, page 330.03, June 2022.

[16] M. Lugaro, U. Ott, and Á. Kereszturi. Radioactive nuclei from cosmochronology to habitability. *Progress in Particle and Nuclear Physics*, 102:1–47, September 2018.

[17] Francesca Matteucci. Modelling the chemical evolution of the Milky Way. , 29(1):5, December 2021.

[18] Francis M. McCubbin, Miriam A. Riner, Kathleen E. Vander Kaaden, and Laura K. Burkemper. Is mercury a volatile-rich planet? *Geophysical Research Letters*, 39(9), 2012.

[19] Andrew McWilliam. Abundance Ratios and Galactic Chemical Evolution. , 35:503–556, January 1997.

[20] Walter Munk and Carl Wunsch. Abyssal recipes II: energetics of tidal and wind mixing. *Deep Sea Research Part I: Oceanographic Research*, 45(12):1977–2010, December 1998.

[21] F. Nimmo, G. D. Price, J. Brodholt, and D. Gubbins. The influence of potassium on core and geodynamo evolution. *Geophysical Journal International*, 156(2):363–376, February 2004.

[22] Francis Nimmo. Why does Venus lack a magnetic field? *Geology*, 30(11):987, November 2002.

[23] Francis Nimmo, Joel Primack, S. M. Faber, Enrico Ramirez-Ruiz, and Mohammadtaher Safarzadeh. Radiogenic Heating and Its Influence on Rocky Planet Dynamos and Habitability. , 903(2):L37, November 2020.

[24] C. O'Neill, Julian Lowman, and Jonathon Wasiliev. The effect of galactic chem-

ical evolution on terrestrial exoplanet composition and tectonics. , 352:114025, December 2020.

[25] V. V. Shimansky, I. F. Bikmaev, A. I. Galeev, N. N. Shimanskaya, D. V. Ivanova, N. A. Sakhibullin, F. A. Musaev, and G. A. Galazutdinov. Observational Constraints on Potassium Synthesis During the Formation of Stars of the Galactic Disk. *Astronomy Reports*, 47(9):750–762, September 2003.

[26] C. Sneden, J. J. Cowan, and R. Gallino. Neutron-capture elements in the early galaxy. , 46:241–288, September 2008.

[27] Diogo Souto, C. Allende Prieto, Katia Cunha, Marc Pinsonneault, Verne V. Smith, R. Garcia-Dias, Jo Bovy, D. A. García-Hernández, Jon Holtzman, J. A. Johnson, Henrik Jönsson, Steve R. Majewski, Matthew Shetrone, Jennifer Sobeck, Olga Zamora, Kaike Pan, and Christian Nitschelm. Chemical Abundances of Main-sequence, Turnoff, Subgiant, and Red Giant Stars from APOGEE Spectra. II. Atomic Diffusion in M67 Stars. , 874(1):97, March 2019.

[28] Lorenzo Spina, Jorge Meléndez, Amanda I. Karakas, Leonardo dos Santos, Megan Bedell, Martin Asplund, Ivan Ramírez, David Yong, Alan Alves-Brito, Jacob L. Bean, and Stefan Dreizler. The temporal evolution of neutron-capture elements in the Galactic discs. , 474(2):2580–2593, February 2018.

[29] Lih-Sin The, Mounib F. El Eid, and Bradley S. Meyer. s-Process Nucleosynthesis in Advanced Burning Phases of Massive Stars. , 655(2):1058–1078, February 2007.

[30] Takuji Tsujimoto. Two Sites of r-process Production Assessed on the Basis of the Age-tagged Abundances of Solar Twins. , 920(2):L32, October 2021.

[31] Cayman T. Unterborn, Jennifer A. Johnson, and Wendy R. Panero. Thorium Abundances in Solar Twins and Analogs: Implications for the Habitability of Extrasolar Planetary Systems. , 806(1):139, June 2015.

[32] G. Wallerstein and H. L. Helfer. Adundances in G Dwarf Stars. II. The High-Velocity Star 85 Pegasi. , 129:720, May 1959.

[33] Peter D. Ward and Donald Brownlee. *Rare Earth: Why Complex Life is Uncommon in the Universe*. Copernicus, 2003.

Appendix A

Ancillary Material

Slopes and Y-intercepts for [Eu/H] vs X Figures			
Dataset/Plot	Slope±error	Y-int±error	Sig
DM Raw thin [Eu/H] vs Age 3.1/3.5	-3.40e-2 ±3.23e-3	1.80e-1 ±1.86e-2	Yes
DM Raw total [Eu/H] vs Age 3.1/3.5	-3.33e-2 ±2.29e-3	1.83e-1 ±1.59e-2	Yes
DM Raw thin [Eu/H] vs [Fe/H] 3.2	7.52e-1 ±1.64e-2	4.11e-2 ±3.71e-3	Yes
DM Raw total [Eu/H] vs [Fe/H] 3.2	6.60e-1 ±1.31e-2	5.04e-2 ±3.86e-3	Yes
DM FeD thin [Eu/H] vs Teff 3.3	-8.85e-5 ±6.36e-6	4.95e-1 ±3.57e-2	Yes
DM FeD total [Eu/H] vs Teff 3.3	-8.85e-5 ±6.74e-6	4.92e-1 ±3.76e-2	Yes
DM 2D(Fe,Teff) thin [Eu/H] vs Age 3.4	-2.22e-3 ±1.26e-3	1.16e-2 ±7.24e-3	No
DM 2D(Fe,Teff) total [Eu/H] vs Age 3.4	2.35e-3 ±9.96e-4	-1.46e-2 ±6.90e-3	No
DM Raw thin [Eu/H] vs [Mg/H] 3.6	7.51e-1 ±2.36e-2	2.76e-2 ±4.83e-3	Yes
DM Raw total [Eu/H] vs [Mg/H] 3.6	7.67e-1 ±1.97e-2	2.12e-2 ±4.50e-3	Yes

Slopes and Y-intercepts for [Eu/H] vs X Figures			
Dataset/Plot	Slope±error	Y-int±error	Sig
DM MgD thin [Eu/H] vs Teff 3.7	-1.14e-4 ±8.47e-6	6.36e-1 ±4.76e-2	Yes
DM MgD total [Eu/H] vs Teff 3.7	-1.17e-4 ±8.00e-6	6.50e-1 ±4.46e-2	Yes
DM 2D(Mg,Teff) thin [Eu/H] vs Age 3.8	-1.34e-2 ±1.54e-3	7.03e-2 ±8.88e-3	Yes
DM 2D(Mg,Teff) total [Eu/H] vs Age 3.8	-1.08e-2 ±1.09e-3	6.68e-2 ±7.55e-3	Yes
BB Raw [Eu/H] vs Age 3.14/3.18	-2.31e-2 ±2.49e-3	1.23e-1 ±2.27e-2	Yes
BB Raw [Eu/H] vs [Fe/H] 3.15	5.76e-1 ±1.48e-2	7.10e-2 ±5.89e-3	Yes
BB FeD [Eu/H] vs Teff 3.16	5.73e-5 ±1.50e-5	-3.31e-1 ±8.69e-2	Yes
BB 2D(Fe,Teff) [Eu/H] vs Age 3.17	2.32e-3 ±1.20e-3	-1.93e-2 ±1.10e-2	No
BB Raw [Eu/H] vs [Mg/H] 3.19	8.05e-1 ±2.24e-2	1.71e-3 ±5.32e-3	Yes
BB MgD [Eu/H] vs Teff 3.20	9.17e-5 ±1.56e-5	-5.30e-1 ±9.01e-2	Yes
BB 2D(Mg,Teff) [Eu/H] vs Age 3.21	-1.01e-3 ±1.25e-3	8.41e-3 ±1.14e-2	No

Table A.1: This Table has all the associated values from the linear fit figures in this document. The Dataset/Plot column is a short descriptor of the relevant plot (will add fig ref) with the corresponding dataset: DM is for Delgado-Mena, and BB is for Battisitini and Bensby. The "Significant" column describes whether or not the linear fit was found to have a p-value less than 0.001. The rows in Red are highlighted as such because they contain information used in the 1D detrend against Teff. The parameters used for the 2D detrending are in Table A.2

2-Dimensional Detrending Parameters			
Dataset/Plot	Y-int	Teff Slope	Metallicity Slope
DM 2D(Fe, Teff) thin [Eu/H] vs Age 3.4	0.549	-9.06e-05	7.82e-01
DM 2D(Fe, Teff) total [Eu/H] vs Age 3.4	0.551	-8.96e-05	6.77e-01
DM 2D(Mg, Teff) thin [Eu/H] vs Age 3.8	0.707	-1.21-04	8.21e-01
DM 2D(Mg, Teff) total [Eu/H] vs Age 3.8	0.701	-1.21e-04	8.18e-01
BB 2D(Fe, Teff) [Eu/H] vs Age 3.17	-0.260	5.73e-05	5.75e-01
BB 2D(Mg, Teff) [Eu/H] vs Age 3.21	-0.529	9.20e-05	8.12e-01

Table A.2: This table lists values that are acquired via a 2D linear fit from the python package sklearn.linear_model with the tool LinearRegression from the package. The Metallicty Slope column describes the slope acquired for the specified Metallicity parameter in the Dataset/Plot column.